



# A lumped kinetic model and experimental investigation of poly(ethylene terephthalate) condensed-phase pyrolysis

A. Locaspi<sup>a</sup>, O. Akin<sup>b</sup>, D. Withoeck<sup>b</sup>, M. Havaei<sup>b</sup>, A. Frassoldati<sup>a</sup>, L. Pratali Maffei<sup>a</sup>, M. Pelucchi<sup>a</sup>, M. Mehl<sup>a</sup>, R.J. Varghese<sup>b</sup>, K.M. Van Geem<sup>b</sup>, T. Faravelli<sup>a,\*</sup>

<sup>a</sup> CRECK Modeling Lab, Politecnico di Milano, Milano 20133, Italy

<sup>b</sup> Laboratory for Chemical Technology, Ghent University, Zwijnaarde 9000, Belgium

## ARTICLE INFO

### Keywords:

Poly(ethylene terephthalate)  
Chemical recycling  
Plastic waste  
Chemical reaction kinetics  
Condensed phase  
Pyrolysis

## ABSTRACT

In a circular economy perspective, plastic waste (PW) is a valuable source of chemicals and energy vectors. Understanding the effect of poly(ethylene terephthalate) (PET) in thermochemical valorisation of complex and contaminated PW mixtures requires definition of suitable kinetic models. This work proposes a condensed-phase semi-detailed kinetic model for PET pyrolysis based on a consolidated functional group approach already validated for other polymers. The reaction network is built considering studies on thermal degradation of PET, model compounds, and small gas-phase esters. Reaction pathways proposed in the scientific literature are critically assessed through analogy with high accuracy gas-phase calculation and are complemented by new proposed pathways. The resulting model couples molecular and radical mechanism and consists of 85 gas and liquid species with 700 liquid-phase reactions, being suitable for CFD simulations of PW pyrolysis upon further reduction. This work also presents new experimental data including TG analysis coupled with GC × GC speciation measurements and elemental characterization of the solid residue. The model is validated by comparison with the new experimental data and a comprehensive set of literature data in terms of characteristic degradation times and detailed product yields. The present work expands the relevant data available for chemistry models development and extends the CRECK kinetic framework for thermochemical recycling of PW mixtures. The proposed kinetic model is attached as [Supplementary material](#) and freely available as an open GitHub repository.

## Nomenclature Abbreviations

Acronym	Description
BDE	Bond Dissociation Energy
CFD	Computational Fluid Dynamics
EC	End-Chain
FG	Functional Groups
FID	Flame Ionization Detector
GC	Gas Chromatography
HMW	High Molecular Weight species
HR	Heating Rate
LMW	Low Molecular Weight species
MC	Mid-chain
MS	Mass spectrometer
MSW	Municipal Solid Waste
PA	Polyamides
PDD	Pulsed discharge ionization detector
PE	Polyethylene

(continued on next column)

## Abbreviations (continued)

Acronym	Description
PET	Poly(ethylene terephthalate)
PMMA	Polymethylmethacrylate
PP	Polypropylene
PS	Polystyrene
PU	Polyurethanes
PVC	Polyvinylchloride
PW	Plastic Waste
RGA	Residual Gas Analyser
SM	<a href="#">Supplementary material</a>
SPU	Supporting Polymer Unit
TCD	Thermal conductivity detectors
TG	Thermogravimetry

## Species nomenclature

(continued on next page)

\* Corresponding author.

E-mail address: [tiziano.faravelli@polimi.it](mailto:tiziano.faravelli@polimi.it) (T. Faravelli).

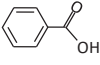
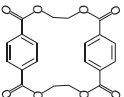
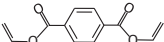
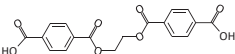
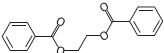
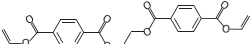
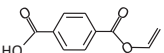
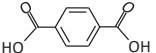
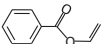
<https://doi.org/10.1016/j.cej.2024.156955>

Received 21 June 2024; Received in revised form 26 September 2024; Accepted 19 October 2024

Available online 22 October 2024

1385-8947/© 2024 The Author(s). Published by Elsevier B.V. This is an open access article under the CC BY license (<http://creativecommons.org/licenses/by/4.0/>).

## Species nomenclature (continued)

Acronym	Description	Representation
Condensable Gas	Species in gaseous form at reaction temperature but condensable at room temperature (tars)	
Gas	Species in gaseous form at reaction temperature	
Light Gas	Species in gaseous form at room temperature	
(L)	Liquid-phase species	
BA	Benzoic Acid	
C	Secondary carbon (-CH <sub>2</sub> -)	
CYEDGE	Cyclic Dimer	
D	Terminal vinyl bond (-C <sub>2</sub> H <sub>3</sub> )	
DVT	Divinyl terephthalate	
EGDA	Ethylene glycol dibenzoic acid	
EGDB	Ethylene glycol dibenzoate	
EGDV	Ethylene glycol divinyl terephthalate	
G-S	Char pseudo-species S	
M	Methyl group (-CH <sub>3</sub> )	
MVT	Monovinyl terephthalate	
Ph	Phenyl ring (-C <sub>6</sub> H <sub>4</sub> -)	
P-S	End-chain species S	
P-S-P	Mid-chain species S	
T	Tertiary carbon (-CH-)	
TA	Terephthalic Acid	
VB	Vinyl Benzoate	

## Mathematical notation

Symbol	Description	Units
A	Modified-Arrhenius frequency factor	cm, mol, s
C <sub>M</sub>	Concentration of monomer	mol cm <sup>-3</sup>
E <sub>act</sub>	Modified-Arrhenius activation energy	cal mol <sup>-1</sup>
h <sub>m</sub>	mass transport coefficient	m <sup>-3</sup> kg <sup>-1</sup> s <sup>-1</sup>
k	Modified-Arrhenius kinetic constant	cm, mol, s
m	Mass	kg
$\dot{m}$	Mass flowrate	kg s <sup>-1</sup>
MW	Molecular Weight	kg kmol <sup>-1</sup>
MW <sub>av</sub>	Number average molecular weight	kg kmol <sup>-1</sup>
n <sub>A</sub>	Modified-Arrhenius temperature exponent	-
r	Molar reaction rate	kmol m <sup>-3</sup> s <sup>-1</sup>
R	Molar formation rate	kmol m <sup>-3</sup> s <sup>-1</sup>
R <sub>g</sub>	Molar gas constant	cal mol <sup>-1</sup> K <sup>-1</sup>
t	Time	s
T	Temperature	K

(continued on next column)

## Mathematical notation (continued)

Symbol	Description	Units
V	Volume	m <sup>3</sup>
γ	CHEMKIN correction parameter	cm <sup>3</sup> mol <sup>-1</sup>
ρ	Density	g cm <sup>-3</sup>

## Scripts

Acronym	Description
0	Initial
av	Average
B	Bubble
b	Bulk
ev	Evaporation
g	Gas-phase
I	Interface
L	Liquid
M	Monomer

## 1. Introduction

Waste valorisation through chemical recycling is a key step towards circular and sustainable chemical and energy industries [1–3]. Poly (ethylene terephthalate) (PET) is among the main constituents of plastic waste (PW) mixtures due to its widespread use in packaging, fibre production, film applications and in the manufacturing and automotive industry [4]. One of the advantages of PET is its higher recycling potential with respect to other plastics through chemical and mechanical processes [5]. Several recycling technologies have been developed in the past decades, but they involve significant purification and separation costs and degrade the material properties [4]. Such issues can be substantially reduced through thermochemical recycling specifically for highly contaminated and complex PW [4,6].

According to the geographical position and seasonality, amounts of PET between 3 to 7 wt% are found in real plastic waste samples [7,8]. Despite this relatively small quantity, the presence of oxygen decreases the quality of pyrolysis oil and may require pretreatment steps [9]. Additionally, the aromatic rings in the backbone enhance the formation of a carbonaceous solid residue (char) that requires further treatment. Most importantly, as previously reported, PET alters the release of chlorinated and nitrogenated compounds from polyvinylchloride (PVC) [10–12] and polyamides (PA) [11,13,14]. As formation of HCl and pollutant release are key issues in PW thermochemical recycling, predicting the degradation of PET and its interactions with other polymers is of paramount importance. Chemical kinetics and fluid dynamics tools can aid both design and optimization of reactors and processes by tailoring the product distribution, release, and energy requirements [7,15].

The thermal degradation of PET has been studied in the scientific literature since the 1950s [16]. From an experimental point of view, the main focus has been given to mass-loss profiles [17–26], while few studies investigated volatile release [17,18,27,28] and char characterization [29–31]. Several research papers have investigated the reaction mechanism appropriately modifying the reaction system or by comparison with similar compounds [16–18,26,29,32–47]. Conversely, the chemical kinetics of these reactions have received low attention in the literature compared to other polymers [48]. Several global kinetic models have been proposed, ranging from simple one-step kinetics to artificial neural networks, proving able to describe polymer mass-loss profiles [14,19,21,23,49–51]. While these models prove flexible for large scale calculations, they do not provide any detail of the reactivity involved [52] and do not allow for extrapolation outside the investigated conditions [7]. To the authors' knowledge, no predictive model able to quantitatively explain the physico-chemical phenomena involved and the observed complex spectra of products has been

developed. Such physics-based models, compared to global ones, provide information also on the modifications of the condensed-phase and volatile release at different operating conditions. Furthermore, they lay the basis for deriving global kinetics representative of the underlying physico-chemical processes [53].

This work proposes a semi-detailed kinetic model for PET condensed-phase pyrolysis. The model builds on previous literature studies [16–18,26,29,32–47] and it is developed following the functional group (FG) approach employed for PVC, polyolefins, and biomass pyrolysis [48,53–56,90]. To aid in model development, a dedicated experimental campaign is performed to assess mass-loss profiles, volatile release, and char characterization. Specifically, new micro-pyrolysis speciation data by comprehensive two-dimensional GC are presented together with elemental characterization of the char residue produced by thermogravimetric (TG) analysis. Model validation is performed also through comparisons with both mass-loss and product distribution experimental profiles from the scientific literature. The resulting condensed-phase model can also be coupled with other subsets describing both solid and gas phase gasification processes to describe secondary reactions and constitutes a first step towards the investigation of mixture interactions in future works.

## 2. Methods and materials

### 2.1. Experimental methodology

A virgin commercial PET sample was employed for all experimental measurements. The elemental CHNS/O composition of the polymer was analysed with a Thermo Scientific FLASH EA2000 analyser (Inter-science, Belgium) operated in combustion mode (ASTM D5291 standard method). Five replicates were performed burning 2–3 mg of sample in pure oxygen at 950 °C. For calibration of the device, a well-defined 2,5-Bis(5-*tert*-butyl-2-benzo-oxazol-2-yl)thiophene (BBOT) standard (Elemental Microanalysis, United Kingdom) was used. An elemental composition of  $62.31 \pm 0.47$  wt% C and  $4.36 \pm 0.08$  wt% H is measured, where no sulphur is detected. Trace amounts of nitrogen ( $0.01$  wt%  $\pm$  5 % rel.) are also measured, likely stemming from nitrogen-containing additives present in low concentrations. Sample oxygen content was determined by difference. The measured elemental composition is in line with the theoretical composition of pure PET (62.5 wt% C, 4.2 wt% H). The same procedure was performed also for char samples.

The pyrolysis experiments were performed by using a single-shot tandem micro-pyrolysis facility (Rx-3050 TR, Frontier Lab., Japan) coupled with a comprehensive two-dimensional Gas Chromatography system (GC  $\times$  GC, Thermo Scientific TRACE Ultra) and a separate multicolumn GC dedicated for analysis of light gases (Thermo Scientific TRACE 1310) equipped with two thermal conductivity detectors (TCD) and a pulsed discharge ionization detector (PDD) described in previous works [57–59]. Briefly, isothermal experiments were performed at 400, 500, and 600 °C dropping 500–800  $\mu$ g of materials into the preheated pyrolysis furnace with a deactivated stainless steel sample cup (Eco-cup LF). The heating rate the sample was subjected to ranges from 100 to 200 °C s<sup>-1</sup> according to the chosen set temperature [60]. The reactor was operated with a He sweep flowrate of 50 mL/min and a pressure of  $\sim$ 2.7 bara. The released volatiles were collected in a cryo-trap (MJT-1035E) cooled with liquid nitrogen and then simultaneously fed to the two analyses systems. The cryo-trap temperature was approximately 77 K, while the holding time was 25 min at 400 °C and 5 min at 500 and 600 °C. The GC columns, an MXT-1 (Restek) non-polar and a ZB-35HT (Phenomenex) polar, were operated from 40 °C to 350 °C with a ramp of 5 °C/min. Compound identification was performed with a BenchTOF-Select™ (Markes, United Kingdom) scanning  $m/z = 50$ –500 at 70 eV comparing the products spectra with the NIST library database. MS spectra of species not reported in the database (e.g., monovinyl and divinyl terephthalate) were identified by comparison with profiles of expected products available in literature [61]. Compound quantification

was performed with a flame ionization detector (FID), calibrated internally with *iso*-butane, and externally using benzoic and terephthalic acid (Sigma Aldrich). The response factors of other compounds were calculated via the molecular response factor (MRF) method as reported by De Saint Laumer et al. [62]. Mass closure obtained from the setup increases with temperature, ranging from 30 % at 400 °C to 70 % at 600 °C. However, considering  $\sim$ 10–30 wt% of solid residue [17,27], and similar results in literature [18,27], the results are deemed acceptable.

TG analysis was performed for both investigating the PET degradation profiles and char quantification, using the NETZSCH STA 449 F3 Jupiter simultaneous thermal analyzer. Grounded PET samples weighing 30–40 mg were loaded into Al<sub>2</sub>O<sub>3</sub> NETZSCH Crucibles (0.3 ml). The analysis was performed under a continuous flow of nitrogen (N<sub>2</sub>) at a rate of 100 mL/min. The initial temperature was raised from 20 °C to specific target temperatures (400 °C, 500 °C, or 600 °C) at a heating rate of 10 °C/min, followed by a 30-minute isothermal period at the set temperature. Further details on all the experimental equipment employed are given in Section S2 of the [Supplementary material](#) (SM).

### 2.2. Physical and mathematical model

The initial polymer is assumed being a small viscous melt approximated as isotropic and homogeneous. Degradation occurs through volumetric liquid-phase reactions that form light liquid-phase compounds able to evaporate. Two sets of equations are introduced for the liquid mass of liquid species  $j$ ,  $m_L^j$ , and for the gas mass of gas species  $k$ ,  $m_g^k$  as:

$$\frac{dm_L^j}{dt} = -\dot{m}_{ev}^j + R_L^j V_L MW_j \quad (1)$$

$$\frac{dm_g^k}{dt} = \dot{m}_{ev}^k + R_L^k V_L MW_k \quad (2)$$

where  $\dot{m}_{ev}^j$  is the evaporation rate of species  $j$ ,  $R_L^j$  its molar liquid-phase formation rate,  $MW_j$  the molecular weight of species  $j$ ,  $V_L$  the liquid volume, and units are kg, kmol, m<sup>3</sup>, s. As mentioned, char species are considered among the liquid-phase set. Thermal equilibrium is assumed between liquid and gas phases and no energy balance equation is introduced. Evaporation rates are evaluated considering mass-transfer resistances of diffusive and convective phenomena [52] as:

$$\dot{m}_{ev}^j = h_m (\rho_j^{l,g} - \rho_j^{b,g}) \quad (3)$$

where  $h_m$  is the average species-independent transport coefficient,  $\rho_j$  are the species densities evaluated at the gas-side interface ( $l,g$ ) and gas-bulk ( $b,g$ ). Equilibrium is assumed at the liquid–vapour interface, and vapour pressures are evaluated from the NIST webbook [63] or employing Nannoolal's group contribution method [64]. Considering average diffusion values of aromatics in N<sub>2</sub> at 400 °C and the typical size of crucibles, the transport coefficient is estimated at  $h_m = 0.1$  m<sup>3</sup>/kg<sub>0</sub>/s. An in-house C++ code based on OpenSMOKE++ [65] was developed to evaluate the sample evolution.

## 3. Kinetic mechanism

The present semi-detailed kinetic model quantitatively describes the condensed-phase chemical phenomena occurring during PET pyrolysis to predict the evolution of the polymer mass and major product distribution at low computational costs. As the degradation mainly occurs above the polymer melting point [47], a molten state for the initial polymer is assumed. The pyrolysis process results in the formation of volatile compounds and a solid residue [66]. In the following, all compounds that evaporate from the molten to the gas phase are defined as “gas species”. Gas species may be light or condensable (tars) gases according to their physical state at room temperature. Conversely, the



carrying similar chemical functionalities. According to the functional groups approach (FG), the reactivity of macromolecules can be described through pseudo-species characteristic of their chemical moieties. The liquid-phase compounds are distinguished in three different subsets: all polymeric chains longer than the trimer are considered High Molecular Weight (HMW) species and are described with functional groups characteristic of the polymer moieties; compounds smaller than the PET trimer are modelled as real species and are referred to as Low Molecular Weight (LMW) species; solid-phase species are described through the fully lumped functional groups approach developed for biochar formation [80].

Each HMW chain is described through a few functional groups representative of mid-chain (MC) and end-chain (EC) moieties as schematically shown in Table 1. The representation of functional groups and the corresponding labels are all shown in Fig. S1 of the SM. All HMW pseudo-species are identified by the initial “P-”, while mid-chains also have a terminal “-P” in their names. HMW species of different chain-lengths are characterized by different amounts of the same functional groups, so that the entire HMW chain-distribution is described through MC and EC pseudo-species only. To identify the chemical moieties of pseudo-species from their names, a specific nomenclature is introduced. “Ph” represents the aromatic rings along the chain ( $-C_6H_4-$ ), while terminal double bonds are labelled “D” ( $-C_2H_3$ ). Alkyl-like carbon atoms are distinguished in methyl groups “M” ( $-CH_3$ ), secondary carbons “C” ( $-CH_2-$ ) and tertiary carbons “T” ( $-CH-$ ). Following this approach, the MC representing the terephthalic moiety ( $-CO-C_6H_4-CO-$ ) is “P-COPhCO-P”, while the glycol moiety ( $-O-CH_2-CH_2-O-$ ) is described by “P-OCCO-P”. The corresponding ECs are “P-COPhCOOH” and “P-OCCOH”. During the degradation process, other groups are formed such as vinyl benzoates, phenyl groups, and aldehydes, and the corresponding pseudo-species are also introduced coherently with the above nomenclature.

The model incorporates alkyl-like, carboxylic, and phenyl radicals to account for the radical degradation. Benzoyl radicals are excluded due to their rapid decarbonylation (i.e., CO release) and the inherent instability of hydrogen atoms in aldehyde functionalities. The presence of a radical is denoted by the dot (“.”) within the label. Certain compounds, such as the ethyl ester end-chain (“P-OCM”), possess two distinct isomer radicals, exhibiting different reactivities. The location of the dot in the species label relates to the type of radical. For example, “P-OCM” represents a primary radical, while “P-OCM” a secondary one.

The evolution of LMW compounds is described similarly to conventional detailed models for pyrolysis of gaseous and liquid fuels [81], employing lumping techniques to reduce the number of species and reactions [82]. Species with boiling temperature ( $T_b$ ) < 200 °C are assumed to directly enter the gas phase upon stabilization (e.g.,

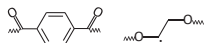
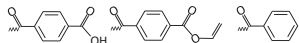
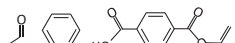
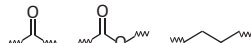
$CH_3CHO$ ,  $C_6H_6$ ) [56]. The degradation products are primarily characterized by phenyl, carboxylic, or vinyl benzoate terminal functionalities. Minor compounds with methyl-ketone or methyl/ethyl ester ends [16] are neglected due to their lower abundance. The same types of radicals considered for HMW species are also introduced for LMW ones. Considering the monomers, all combinations of terminal functional groups are explicitly considered. For example, the model includes three monomers with one carboxylic end, namely benzoic acid (BA) for phenyl-carboxylic ends, monovinyl terephthalate (MVT) for vinyl-carboxylic ends, and terephthalic acid (TA) for carboxylic-carboxylic ends. As regards dimers, cyclic dimers (CYEGDE) and symmetric configurations are considered. The latter include ethylene glycol dibenzoate (EGDB), ethylene glycol divinyl terephthalate (EGDV), and ethylene glycol dibenzoic acid (EGDA), while mixed configurations are represented as their combination. The structure of monomers and dimers introduced in the model are represented in Fig. S2 of the SM, except for the cyclic ones for clarity purposes.

As the degradation proceeds, formation of polycyclic aromatic hydrocarbons and subsequent dealkylations and decarbonylations result in the formation of a carbonaceous solid residue (char). While coal- and bio-char have been significantly studied in the past decades [55,83,84], to the authors’ knowledge, few characterization data are available for plastic char. Specifically, several studies focused on char yield from PET, but few elemental characterizations have been performed in controlled conditions [29,30,85–87] despite their relevance in evaluating char reactivity and its secondary reactions [84]. The current mechanism employs the fully lumped approach developed for biochar formation [55] introducing the corresponding species and reactions. A single species labelled CHAR describes the aromatic structure, together with pseudo-species representative of ketone, ether, ester, aliphatic, and other moieties. The names of these compounds start with the “G-” label (e.g., G-CO, G- $H_2$ ) and represent the evolution of char’s elemental composition. Since the reference biomass model is fully lumped, the radical reactivity is lumped in reactions representative of the global behaviour of pseudo-components. For instance, phenyl hydrogens are represented by the G- $H_2$  species, and a single unimolecular reaction represents its release to  $H_2$ . Similarly, methyl bridges and toluene-like structures are represented through the species G- $CH_4$  which decomposes in a single lumped step to gas-phase  $CH_4$ . Overall, the char pseudo-species share the same chemical composition as the stable gas-phase molecules they decompose into [55,80,88,89].

The total number of liquid-phase pseudo-species (Table 1) introduced to describe PET condensed-phase degradation is 51, 18 of which are HMW species. Liquid-phase species are identified by “(L)” and the same LMW species are present also in the gas phase, obtaining a total number of 84 species.

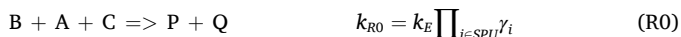
**Table 1**

Schematic representation of the HMW, LMW, and char species introduced for PET degradation.

Species	Stable	Radical	Representation of main species
HMW MC	3	3	
EC	6	6	
LMW	9	16	
Char	8	–	
Number of liquid species	51		
Number of gas species	33		

### 3.2. Developing a CHEMKIN-format reaction mechanism with the functional groups approach

The functional groups (FG) approach describes the reactivity of fragments of the polymeric chains. Compared to real species, reactions of these pseudo-species may affect the neighbouring fragments, either modifying their chemical bonds or their location within the polymer chain. The concept of supporting polymer unit (SPU) is introduced to represent these phenomena [56,90]. The present Section presents a generalization of the SPU formulation, while Section 3.3.1 shows a practical example within the context of PET pyrolysis. In general, consider three neighbouring chain fragments “A”, “B”, and “C” forming a sequence “B-A-C” along the chain. In this sequence, “A” is the mid chain species, while “B” and “C” can be either mid-chain or end-chain species. The fragment “A” can undergo a generic unimolecular elementary step “E” with an elementary rate constant “ $k_E$ ”. Following the FG approach, the model introduces a reaction “R0” that forms two products “P” and “Q” as:



where  $k_{RO}$  is the reaction rate constant of “R0”, “B” and “C” are the SPU of the reaction, and  $\gamma_i$  correction factors discussed in Eq. (4). This reaction appears as a termolecular reaction since the fragments are represented by three different pseudo-species. The type of products depends both on the reaction and on the type of SPUs. For instance, if “B” and “C” are mid-chain species and “E” is a chain-shortening reaction, “P” and “Q” are two end-chain species. Conversely, if one of the SPUs is an end-chain species, reaction “R0” forms LMW products. The transformation of MCs into ECs and ECs into LMW species represents the decrease of the polymer chain length. Overall, the difference between reactants and products lies in the functionality of the chains, described by the type of fragments, and in their different chain-lengths, characterized by the ratio of MCs to ECs. The methodology also considers the opposite process, i.e., bimolecular reactions such as radical addition or recombination forming mid-chain species from two end-chain reactants, representing the increase of the average chain length.

The same elementary reaction “E” can also occur in the presence of other SPUs. Following the CHEMKIN format, the model introduces a separate reaction for all relevant SPUs that can be employed by the reactive site. From a kinetic perspective, the SPUs do not affect the elementary reaction rate ( $r_E$ ) as they are required only to preserve the physical interpretation of the fragment degradation, hence their definition of “spectators”. However, the rates of the different reactions with SPUs must account for the relative amount of SPU available to the polymer. To avoid modifying the total reaction rate of “A”, this dependence should follow the amounts of each SPU compared to all the available SPUs. This dependence can be included within the numerical solver, but it is not CHEMKIN-format compliant. To incorporate “a priori” a dependence of the reaction rate in the fraction of SPU, the kinetic constant employed in the model ( $k_{RO}$ ) is obtained modifying the elementary kinetic constant  $k_E$  as shown in “R0”. Specifically, for each SPU “i” introduced in the reaction, the constant is modified by a species-dependent parameter  $\gamma_i$ . This modifier is based on the concentration of species  $i$  ( $\rho_L/MW_i$ ) and the total amount of SPU available at the initial time as:

$$\gamma_i = \frac{MW_i}{\rho_L} \frac{1}{\sum_{j \in SPU_E} \omega_j^0} \quad (4)$$

where  $\rho_L = 1.4 \text{ g cm}^{-3}$  is the mixture density (assumed constant in the liquid phase),  $MW_i$  is the molecular weight of species  $i$ , and  $\sum_{j \in SPU_E} \omega_j^0$  is the sum of initial SPU mass fractions ( $\omega_j^0$ ) that may be involved in reaction “E” ( $SPU_E$ ). Because of these corrective terms, the frequency factors of the reactions in the model differ from the values of the elementary steps reported in the following sections. The proposed correction is CHEMKIN-format compliant, and it allows to introduce a dependence on the mass fraction of the support species  $i$  as:

$$r_{RO} = \left( k_E \prod_{i \in SPU} \gamma_i \right) C_A \prod_{i \in SPU} C_i = k_E C_A \prod_{i \in SPU} \frac{\omega_i}{\sum_{j \in SPU_E} \omega_j^0} \quad (5)$$

This correction introduces several approximations. Firstly, as mentioned, the required dependence is on the molar fraction of the SPU

**Table 2**  
Modified-Arrhenius parameters for the rate constants of molecular elementary reactions (units cm, mol, s, cal).  $k = A T^{n_A} \exp(-E_{act}/R_g T)$ .

Reaction	A	$n_A$	$E_{act}$
(R1) Syn elimination	$3.0 \times 10^{12}$	0	48,000
(R2) Assisted molecular decarboxylation	$8.0 \times 10^{09}$	0	36,000
(R3) Carboxylic acid dimerization	$5.0 \times 10^{10}$	0	35,000
(R4) Vinyl ester isomerization	$2.0 \times 10^{13}$	0	50,000
(R5) Ester-interchange	$1.0 \times 10^{06}$	0	20,000
(R6) Pseudo Diels-Alder	$1.0 \times 10^{07}$	0	35,000

**Table 3**

Modified-Arrhenius parameters for the rate constants of radical elementary reactions (units cm, mol, s, cal).  $k = A T^{n_A} \exp(-E_{act}/R_g T)$ .

Reaction	A	$n_A$	$E_{act}$
(R7) Random scission OC-CO	$6.0 \times 10^{14}$	0	74,000
(R8) H-abstraction of $R_{OCCO}$ on $H_{OCCO}$	$3.0 \times 10^{11}$	0	13,500
(R9) $\beta$ -scission COO-C	$5.0 \times 10^{12}$	0	32,000
(R10) $\beta$ -scission CO-OC	$2.0 \times 10^{13}$	0	36,000
(R11) Radical decarboxylation	$5.0 \times 10^{13}$	0	16,000
(R12) Glycol 1–5 isomerisation	$5.0 \times 10^{10}$	0	26,000
(R13) Alkyl-like carbonyl addition	$5.0 \times 10^{09}$	0	11,000
(R14) Alkyl-like aromatic addition	$2.0 \times 10^{10}$	0	18,000
(R15) Phenyl carbonyl addition	$5.0 \times 10^{09}$	0	2,000
(R16) Phenyl aromatic addition	$2.0 \times 10^{10}$	0	6,000
(R17) Radical recombination	$1.0 \times 10^{08}$	1	11,000

compared to the total molar fractions of all SPUs available ( $x_i/\sum_{j \in SPU} x_j$ ). Since the mixture molar composition changes with the reaction, correctly accounting for both concentrations and SPU molar fractions requires hard coding the reaction rate expression. The most sensitive assumption is that the mass fractions in Eq. (5) are normalized on the initial mass fractions of the SPU. The error is negligible for polyolefins, whose liquid-phase composition is dominated by the polymeric species, while errors are introduced due to the description of char formation in PET degradation. Specifically, formation of CHAR(L) results in a dilution effect on the reaction rate as it is considered a liquid species to avoid considering a ternary system (gas-liquid-solid phases). As mentioned, the value of  $\sum_{j \in SPU_E} \omega_j^0$  in Eq. (5) is set a priori and it does not vary with the composition of the condensed phase. Conversely, formation of species not involved in SPU reactions (e.g., CHAR(L)) result in a decrease of both  $C_A$  and  $\prod \omega_i$ , which corresponds to a reduction of the reaction rate with respect to the elementary step ( $k_E C_A$ ). On the one hand, char decreases the available reactive volume [83], but Eq. (5) indirectly introduces a dependence in its formation related to the number of SPU introduced. To counteract the over-dilution effect caused by char formation in the present formulation, the frequency factor of reactions that employ end-chains as SPUs is increased by 2 per EC introduced. Indeed, reactions employing ECs as SPU are favoured in the later stage of the degradation, i.e., when char becomes among the main liquid-phase species. The error resulting from the approximation of Eq. (5) varies with polymer conversion, but it has a mild impact on the overall model predictions. When compared to the ternary system model, this translates in smoother mass-loss profiles at  $m_L < 30\%$  with a maximum discrepancy of  $\sim 3 \text{ wt\%}$  occurring at  $m_L \sim 22\%$ . Product yields are also affected, resulting in a decrease of  $\sim 1 \text{ wt\%}$  for yields of products characteristic of the molecular degradation mechanism (i.e., MVT, DVT, TA, EGDV, EGDA). The rate constants reported in Tables 2 and 3 implicitly account for these phenomena. Developing an analogous model for the ternary system requires slight corrections to the kinetic constants, which are however well within the uncertainty involved in their estimation.

### 3.3. Molecular degradation mechanism

The importance of concerted molecular reactions has been highlighted in the degradation of both PET [16,33,34,37,38] and of small gas-phase esters [63,67,73,91]. Table 2 summarizes the considered molecular reaction classes with their modified-Arrhenius parameters. The proposed kinetic parameters represent, in a lumped fashion, complex molecular scale phenomena, and interface cracking effect [92]. Each family of reactions and the corresponding kinetics are discussed in the following paragraphs. Due to space limitations, some reactions are schematically represented in Section S1 of the SM. The labels reported in Table 2 refer to the elementary reaction class, while reactions derived from the elementary ones are labelled adding letters to the class number (e.g., R1a, R3c, etc). These molecular reactions are introduced also for

LMW species with  $T_b > 200$  °C. For instance, dimers can decompose to monomers through syn elimination reactions, and monomers can further decompose through decarboxylation or vinyl isomerization.

### 3.3.1. Syn elimination

Molecular cleavage and rearrangements of PET units can occur through a concerted 6-center syn elimination with hydrogen transfer (R1). The reaction is schematically shown in Fig. 2, where mid-chain species are represented in blue, end-chains in red, and SPUs are identified by the dashed lines. Fig. 2.a shows the syn elimination reaction occurring employing the MC units as SPU, while Fig. 2.b shows the same reaction employing one MC and one EC units as SPU. Considering reaction R1a, the initial glycol and terephthalic mid-chain species get converted to a carboxylic (P-COPhCOOH) and a vinyl benzoate (P-COPhCOOD) end-chain. As discussed in Section 3.2, the glycol unit (P-OCCO-P) is the reactive site, while the two neighbouring terephthalic MC units (P-COPhCO-P) are employed as SPU [56,90]. The reaction is first order in the concentration of the glycol mid-chain, and the elementary kinetic constant is modified introducing a  $\gamma_i$  correction (Eq. (4)) per each SPU. The correction term  $\gamma_i$  for the terephthalic mid-chain unit (P-COPhCO-P) is estimated as  $\gamma_{P-COPhCO-P} = 132/1.4/0.7 \text{ cm}^3 \text{ mol}^{-1} = 134 \text{ cm}^3 \text{ mol}^{-1}$ , where  $MW_i = 132 \text{ g mol}^{-1}$ ,  $\rho_L = 1.4 \text{ g cm}^{-3}$ , and  $\sum_{j \in SPU_{R1}} \omega_j^0 = \omega_{P-COPhCO-P}^0 = 0.7$ . The latter term accounts for all units that can be employed as SPU by the glycol units in the syn

elimination reaction, which at the initial time are only the terephthalic MC. Considering PET pyrolysis, reactions employing the terephthalic unit as SPU do not employ the glycol one and vice versa, and therefore  $\sum_{j \in SPU_E} \omega_j^0 < 0$ . The frequency factor of reaction R1a ( $A_{R1a}$ ) is evaluated from the value reported in Table 2. As two SPU are introduced in the reaction, the resulting value is  $A_{R1a} = A_{R1} \times \gamma_{P-COPhCO-P} \times \gamma_{P-COPhCO-P} = 3.0 \times 10^{12} \times 134^2 \text{ cm}^6 \text{ mol}^{-2} \text{ s}^{-1} = 5.4 \times 10^{16} \text{ cm}^6 \text{ mol}^{-2} \text{ s}^{-1}$ . Due to the presence of two SPUs, the reaction constant employed in the mechanism has the units of a termolecular reaction.

As the mid-chain units are consumed, the probability of having short chains with neighbouring EC functionalities increases. For instance, Fig. 2.b shows the reaction involving one MC and one EC unit as SPU (R1b). R1a and R1b derive from the same elementary reaction class R1, but only R1b results in formation of LMW products. The formation of both monomers and dimers is lumped in a single step, utilizing the sum of the stoichiometric coefficients of the elementary steps [81]. The equal probability to form either a carboxylic or vinyl end on the polymer is reflected by the corresponding end-chains in the product distribution. Similarly, the LMW species can have either two acid ends or a combination of one benzoic and one vinyl end. Dimers with different terminations are represented as 0.5EGDA and 0.5EGDV. The reaction is developed analogously to R1a, where the frequency factor of R1 is modified introducing  $\gamma_{P-COPhCO-P} = 134 \text{ cm}^3 \text{ mol}^{-1}$  and  $\gamma_{P-COPhCOOH} = 149/1.4/0.7 \text{ cm}^3 \text{ mol}^{-1} = 152 \text{ cm}^3 \text{ mol}^{-1}$ . The denominator is the same

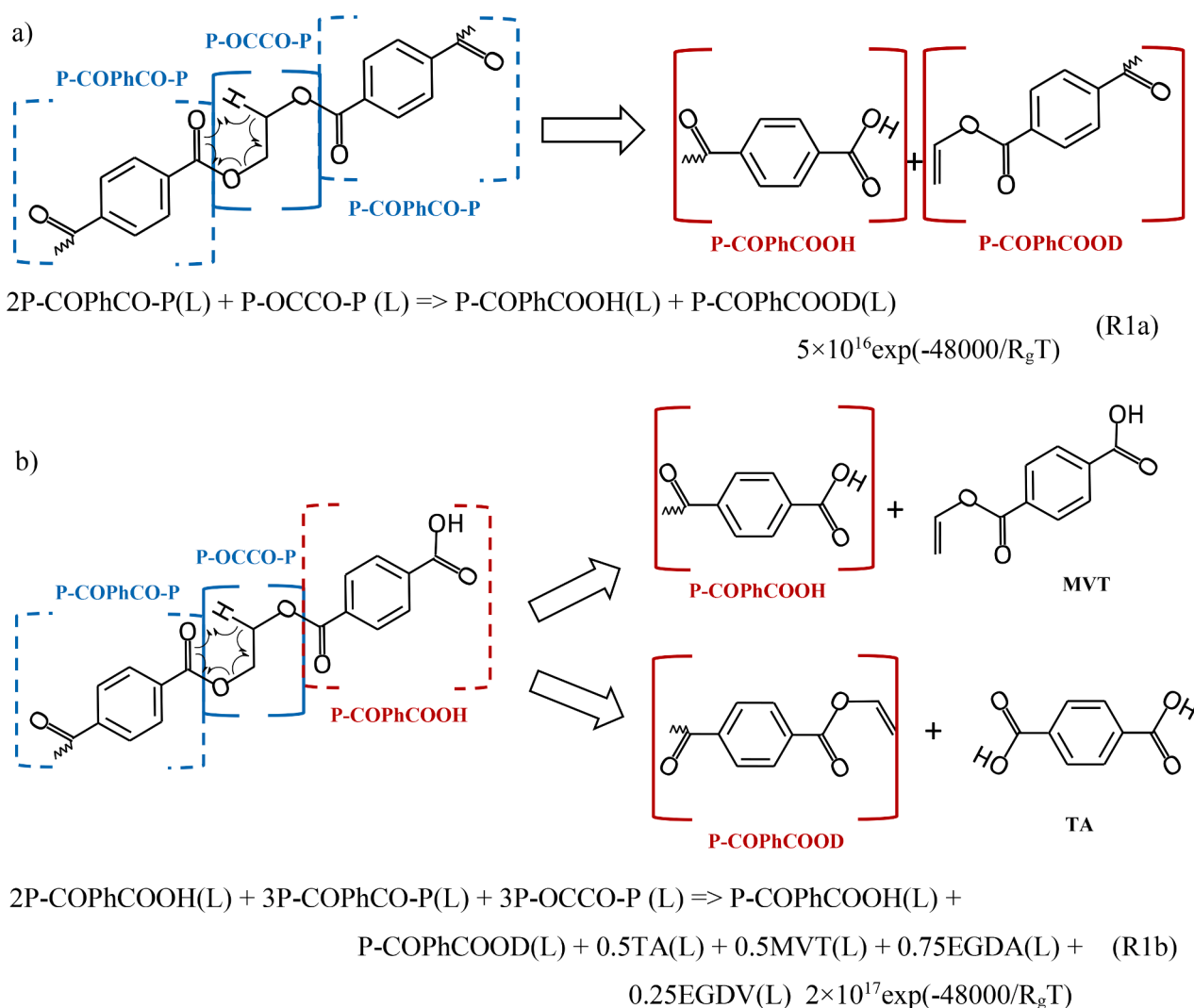


Fig. 2. Representation of the syn elimination reaction employing as SPU (dashed lines): a) two mid-chain units to form end-chains; b) a mid-chain and a carboxylic end-chain units releasing volatiles and end-chains. Species nomenclature employs Ph for  $-C_6H_4-$ , C for  $-CH_2-$ , and D for  $-C_2H_3$ .

for both  $\gamma_i$  as  $\sum_{j \in \text{SPUR}_i} \omega_j^0 = 0.7$  for both situations. The frequency factor of reaction R1b is then evaluated as  $A_{R1b} = 2 \times A_{R1} \times \gamma_{P-COPhCO_2-P} \times \gamma_{P-COPhCOOH} = 2 \times 3.0 \times 10^{12} \times 134 \times 152 \text{ cm}^6 \text{ mol}^{-2} \text{ s}^{-1} = 2 \times 10^{17} \text{ cm}^6 \text{ mol}^{-2} \text{ s}^{-1}$ , where the factor of 2 is introduced to counterbalance the over-dilution caused by char formation (Section 3.2). The model introduces also reactions employing two end-chains as SPU which release only LMW. As these reactions employ 2 ECs as SPU, the frequency factor is further increased by a factor of 2 compared to reaction R1b. The same syn elimination reaction can also occur on glycol end-chains releasing  $\text{CH}_3\text{CHO}$  and a carboxylic end-chain.

The kinetic parameters of the syn elimination R1 are defined by analogy to gas-phase ethyl esters [63,73,91,93]. Since the C-H bond in  $\alpha$  to the ester is more labile than a primary hydrogen, an activation energy of 48 kcal/mol is introduced. Huang et al. [34] calculated a gas-phase energy barrier of 43 kcal/mol for the PET dimer, which is 7 kcal/mol lower than the barrier of ethyl metanoate [63,73,91,93], possibly due to the weaker C-H bond or also to the low-accuracy DFT method employed. Ma et al. [42] studied free energy surfaces of PET dimers at 435 °C, suggesting that this concerted pathway has comparable rates to the homolytic C-C bond fission (discussed in detail in Section 3.4.1). However, at  $T < 700$  °C initiation reactions affect polymer degradation only in terms of total radical concentration [81,94], while propagation reactions control the product selectivity. Therefore, the results of Ma et al. [42] imply that molecular pathways do not significantly affect PET pyrolysis, in contrast with the rest of the scientific literature. In the present work, compared to R1, syn elimination on glycol ECs employs a 3 kcal/mol decrease in activation energy due to the lower BDE of the C-H bond  $\alpha$  to an OH group [78,95].

The thermal degradation forms ethylidene structures as discussed in Section 3.4. This ethylidene diester (P-OTMO-P) also undergoes decomposition through two kinds of 6-centered molecular pathways. The first one is analogous to the syn elimination shown in Fig. 2. This path forms the same benzoic and vinyl ECs, and also involves all combinations of ECs and MCs as SPU. Compared to reaction R1a, a 2 kcal/mol increase in  $E_{\text{act}}$  is considered because of the higher BDE of primary hydrogens [63]. The frequency factor is assumed 3 times higher because of the lower steric hindrance and the higher number of hydrogens. The alternative degradation pathway for the ethylidene diester involves interaction between the oxygen and carbon atoms of the two carbonyl groups (R1c). This reaction occurs through a 6-membered ring and forms  $\text{CH}_3\text{CHO}$  and an anhydride moiety as shown in Fig. 3. Carson et al. [96] estimate a BDE of  $\sim 75$  kcal/mol, but this value is 20 kcal/mol lower than smaller analogous anhydrides [63,78] and estimates from other studies [97,98]. The phenyl anhydride lacks available hydrogens compared to small analogues and it reacts more slowly, only by chain initiations, radical additions, or hydro/alcoholysis. Hence, the

anhydride of R1c is represented through char pseudo-species, and the two outer phenyl ketone moieties are represented as half terephthalate MCs. To avoid introducing additional char species with respect to the biomass model [99],  $\text{CO}_2$  is directly released. The remaining oxygen atoms are represented as G-CO and G-CO $_2$  to account for the partial release of CO and the remaining oxygen being trapped within the char matrix. The aromatic carbon and hydrogen are represented by G-H $_2$  and CHAR species. The Arrhenius parameters for this reaction are also similar to the glycol syn elimination. However, compared to R1 a 6 kcal/mol decrease in  $E_{\text{act}}$  is introduced to account for the polarization of the carbonyl groups. Conversely, the frequency factor is 25 times lower because of the higher steric hindrance of the bulky aromatic groups. A single MC is employed as SPU as the second one is also present as a product and therefore cancels out.

### 3.3.2. Molecular decarboxylation and dimerization

The main products of syn eliminations are carboxylic and vinyl ends. Molecular pathways are considered for both functionalities. Several studies on gas-phase molecular decarboxylation are reported in the scientific literature [63,73,100,101]. These reactions have similar frequency factor as syn elimination, but 10–15 kcal/mol higher  $E_{\text{act}}$ , and are therefore not relevant at the conditions typical of PET degradation. Conversely, the carboxylic acids catalysed decarboxylation reaction (R2) [35,98,102,103] is considered, introducing an additional P-COPhCOOH(L) unit as a catalyst not consumed across the reaction (Fig. S3 of the SM). Similar reactions are introduced to account for end-chains catalysing dimers and monomer decomposition and vice-versa. Because of the low liquid-phase concentrations, interactions between LMW compounds are neglected to simplify the mechanism. An activation energy of 35 kcal/mol is considered for reaction R2 in line with the one reported by Liu et al. [98]. The frequency factor is instead adopted by analogy to the gas-phase addition of a carboxylic acid to a vinyl bond [73] and to Diels-Alder kinetics in PVC pyrolysis [54]. The model considers also acid dimerization/dehydration to form the corresponding anhydride (R3). This reaction is similar to the catalysed decarboxylation, but it consumes both moieties to form water. The anhydride product is represented as in reaction R1c. This work employs the energy barriers proposed by Liu et al. [98], with a 1 kcal/mol decrease compared to bimolecular decarboxylation. The frequency factor is assumed  $10^{0.8}$  times larger than that of bimolecular decarboxylation. This difference is introduced because of the smaller (6-member) transition state of dimerization compared to the 7-member state of assisted decarboxylation [104].

### 3.3.3. Vinyl ester isomerization and molecular decomposition

Vinyl benzoate ends can undergo various reaction pathways similar

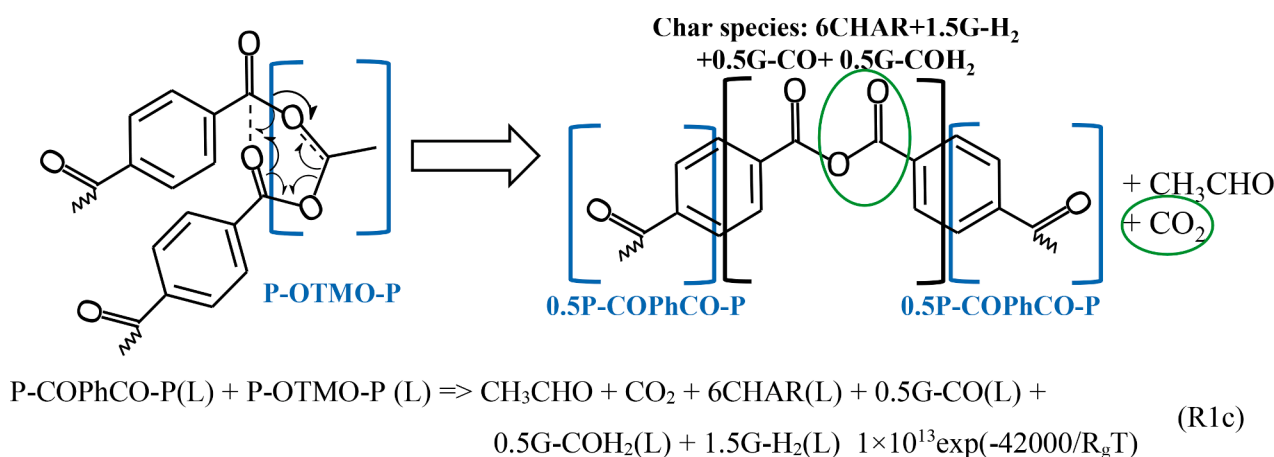


Fig. 3. Schematic representation of the ethylidene syn elimination to form phenyl anhydride and acetaldehyde. Species nomenclature employs Ph for  $-\text{C}_6\text{H}_4-$ , C for  $-\text{CH}_2-$ , T for  $-\text{CH}-$ , M for  $-\text{CH}_3$ , and D for  $-\text{C}_2\text{H}_3$ .



to those observed for vinyl acetate [16,75,91]. The analogous syn elimination (R1) is excluded due to the higher BDE involved compared to primary hydrogens (~10 kcal/mol [78]). The model considers only their primary unimolecular decomposition pathway (R4), which involves a rearrangement to form a  $\beta$ -keto-aldehyde (benzoylacetaldhyde) that decomposes forming CO and an acetophenone moiety [16] (Fig. S4 of the SM). Since the rate-determining step for the vinyl ester molecular degradation is the intramolecular rearrangement, the reaction products are represented through the main compounds derived from acetophenone pyrolysis (i.e., ketene and phenyl rings by radical degradation), with the additional benefit of avoiding an increase in the model size. The rate parameters for the rate-determining step are based on the analogous gas-phase keto-enol tautomerization [105]. The activation energy is lowered by 2 kcal/mol due to the polarization of the carbon atom in the carbonyl group. These parameters involve higher temperatures compared to those proposed by Morsch et al. [91] for vinyl acetate, which were adjusted to match the selectivity data reported by Allan et al. [44].

### 3.3.4. Ester-interchange reactions

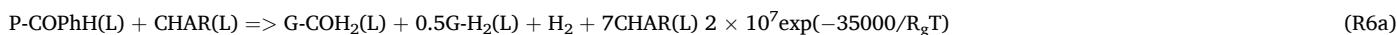
Glycol end-chains can participate in alcoholysis reactions (R5) with both mid-chain and end-chain moieties. These reactions affect the initial stages of degradation and under conditions of low initial molecular weight. Reactions occurring near the end-chain itself result in formation of cyclic dimers (CYEDGE) as:



where the glycol end-chain is not consumed across the reaction. The reaction is bimolecular in the concentration of P-OCCOH(L) and P-COPhCO-P(L) and employs the glycol unit as SPU. Although ester alcoholysis is a well-studied reaction, the existing kinetic analyses primarily focus on acid and base catalysis within specific solvents. For the present purposes, the kinetic parameters proposed by Reimschuessel et al. [103] are considered. The same reaction can take place on the vinyl end to release acetaldehyde and regenerate the initial polymer moiety. Bimolecular alcoholysis can take place also on the carbonyl group near the end-chains releasing LMW products.

### 3.3.5. Pseudo-Diels-Alder reactions

Diels-Alder reactions result in condensation and growth of polycyclic aromatic carbons and are the only considered pathways that involve interaction of HMW and LMW species with the char functional groups. For instance, phenyl end-chains get embedded in the char structure according to the following reaction:



As regards kinetic parameters for R6, the activation energy is the same as proposed by Marongiu et al. [54] for Diels-Alder reactions occurring in PVC pyrolysis. However, the pre-exponential factors are significantly different due to the unique reaction context. In this case, the reaction involves the molecular addition to an aromatic network within the char, where CHAR is represented by a single carbon atom. This description through the CHAR species leads to high carbon

concentrations, but it also neglects the fact that only the surface layer of the aromatic network is actually accessible [84,106]. Overall, to represent these phenomena, an adjusted pre-exponential factor of  $10^7 \text{ cm}^3 \text{ mol}^{-1} \text{ s}^{-1}$  is employed. The frequency factor of R6a is 2 times higher than the elementary step to account for the higher available surface for the charification reaction.

## 3.4. Radical degradation mechanism

The radical degradation is responsible for formation of CO, CH<sub>3</sub>CHO, and polycyclic aromatic structures. These pathways are dominant at higher temperatures, but also affect product distributions at lower T (e.g., char and CO<sub>2</sub> formation). The mechanism is schematically represented in Fig. 1 and described in greater detail in the following paragraphs. Table 3 reports the considered elementary reactions and the corresponding modified-Arrhenius parameters. Initiation occurs by random scission, and the produced radicals then undergo propagation reactions such as H-abstractions,  $\beta$ -scissions, and radical additions. Only termination by radical-radical recombination is considered. As with PVC [54] and lignin [107], condensation and radical additions to the aromatic rings result in formation of considerable amounts of char (10–20 wt%). The onset temperatures are mainly affected by  $\beta$ -scissions, which are the rate determining step, and random scission and recombination reactions, which control the radical pool. H-abstractions and additions control the product distribution together with  $\beta$ -scissions

reactions.

The propagation reactions introduced for HMW pseudo-species are also defined for LMW molecules. For instance, terephthalic acid radicals (T $\dot{\text{A}}$ ) can decarboxylate to phenyl radicals of benzoic acid (B $\dot{\text{A}}$ ), which then stabilize. Small radicals such as  $\dot{\text{C}}_2\text{H}_3$  and  $\dot{\text{C}}\text{H}_2\text{CHO}$  are explicitly considered together with their decomposition reactions, but once stabilized the molecules are assumed to not undergo further reactions because of their fast evaporation. On the other hand, for molecules with higher boiling points, secondary reactions of the stable molecules are considered due to their lower evaporation rates. For instance, the present mechanism includes H-abstractions from monovinyl terephthalate (MVT) to form the carboxyl radicals (MV $\dot{\text{T}}$ ) and their decomposition to vinyl benzoate radicals (VB $\dot{\text{B}}$ ). Similarly, radical additions to vinyl benzoate forming light products and end-chains and char species are included as well.

### 3.4.1. Radical initiation reactions

Initiation occurs via random scission of the C-C bonds within the

glycol moiety (R7) [34,42], which produces two methyl ester radicals (Fig. S5 of the SM). The rate parameters are estimated through several analogies with gas-phase compounds and the transposition from gas to liquid. Considering a gas-phase PET dimer, Huang et al. [34] compute a BDE of 81 kcal/mol, which is 6 kcal/mol lower than typical values for normal alkanes and gas-phase ethyl esters [63,67,78,93,95]. In the present work, the introduced gas-phase energy barrier of PET is 2 kcal/mol lower compared to n-alkanes, due to the electron-withdrawing effect of the neighbouring oxygen atoms [95]. The proposed difference in

gas-phase  $E_{\text{act}}$  between initiation and syn elimination is 31 kcal/mol, aligning with the differences in energy barriers proposed by Huang et al. [34]. To account for the transition of gas-phase reactions to the liquid phase, the solvation correction proposed by Ranzi et al. [94] is employed. This correction applies to reactions with a reverse step characterized by low activation energies [76]. A decrease of 5 kcal/mol is estimated from viscosity values reported by Van Krevelen [108]. As with the molecular reactions, different SPUs are considered introducing appropriate corrections (Section 3.2). To simplify the mechanism, the radical pool is assumed controlled only by HMW species, as the liquid-phase reactivity of LMW species is characterized mainly by propagation reactions and their phase-change rate.

Vinyl esters significantly contribute to the radical pool in PET degradation. As highlighted by Morsch et al. [91] and in-line with the BDEs computed from the ATcT and NIST databases [63,78], the CO-O bond in vinyl esters is 24 kcal/mol weaker than that in esters without vinyl groups. This difference arises from the formation of the resonantly stabilized ethenol radical ( $\dot{\text{C}}\text{H}_2\text{CH}_2\text{O}$ ), while the aromatic ring has negligible increase in its resonance stabilization due to the non-planarity of the unpaired electron of benzoyl. Initiation reactions on the CO-O bond are introduced assuming that the benzoyl radical readily decarboxylates and the acetaldehyde radical stabilizes and evaporates immediately (Fig. S6 of the SM). The BDE for this scission is similar to allylic initiation, and the same selectivity of gas-phase hexene is employed [109]. The proposed values are quite in good agreement with the difference in energy barriers estimated by Huang et al. [34]. Vinyl ester moieties are also the primary products of the molecular degradation mechanism, resulting in the radical mechanism being enhanced by the molecular one. LMW vinyl esters are the only species considered to affect the total radical pool because of their high initiation rate.

### 3.4.2. H-abstraction reactions

The radicals formed by initiation undergo different propagation

reactions according to their reactivity. As mentioned, the present mechanism considers primary and secondary alkyl-like radicals, benzoyloxyl radicals, and phenyl radicals. All radicals participate in H-abstraction reactions (R8), with the selectivity proposed by Ranzi et al. [110]. H-abstractions to form vinyl radicals are not included [76], while those on phenyl hydrogens are considered due to their large amounts and the importance of radical addition pathways. Phenyl radicals stabilize rapidly, but at  $T < 500^\circ\text{C}$  aromatic and carbonyl additions have rates similar to the H-abstraction reactions.

### 3.4.3. $\beta$ -decomposition reactions

The most abundant radical within the system is the mid-chain glycol radical (P-O $\dot{\text{C}}\text{CO}$ -P). This species decomposes following two  $\beta$ -scission routes (R9-R10) as shown in Fig. 4. The first pathway (R9a) breaks the COO-C bond and forms a vinyl ester and a benzoyloxyl radical (Fig. 4.a). The energy barrier of this reaction is evaluated based on the analogous one in PE pyrolysis [53]. Overall, an increase of 4 kcal/mol is considered due to two factors. Firstly, the stabilizing effect of the ester group in the reactant increases the BDE by 2 kcal/mol, as computed by small gas-phase analogues [78]. Secondly, the COO-C bond within the ester group of the product is 2 kcal/mol stronger than that in typical alkyl radicals [78]. The second class of  $\beta$ -scission reactions involves breaking the CO-OC bond to form a benzoyl radical and an aldehyde that decarboxylates releasing CO (R10a in Fig. 4.b). The  $\beta$ -ester-aldehyde product is represented through its main decarbonylation products, i.e., CO and a methyl ester. The competition between the two  $\beta$ -scission reactions affects the high temperature CO/CO<sub>2</sub> ratio. A selectivity similar to the one proposed for unsaturated ethyl esters by Bennadji et al. [93] is employed, resulting in the second pathway being most relevant at high temperatures.

Fig. 5 shows additional  $\beta$ -scission reactions considered in the present mechanism. The first one is decarboxylation of benzoyloxyl radicals (R11), which is the main responsible for CO<sub>2</sub> release. The considered

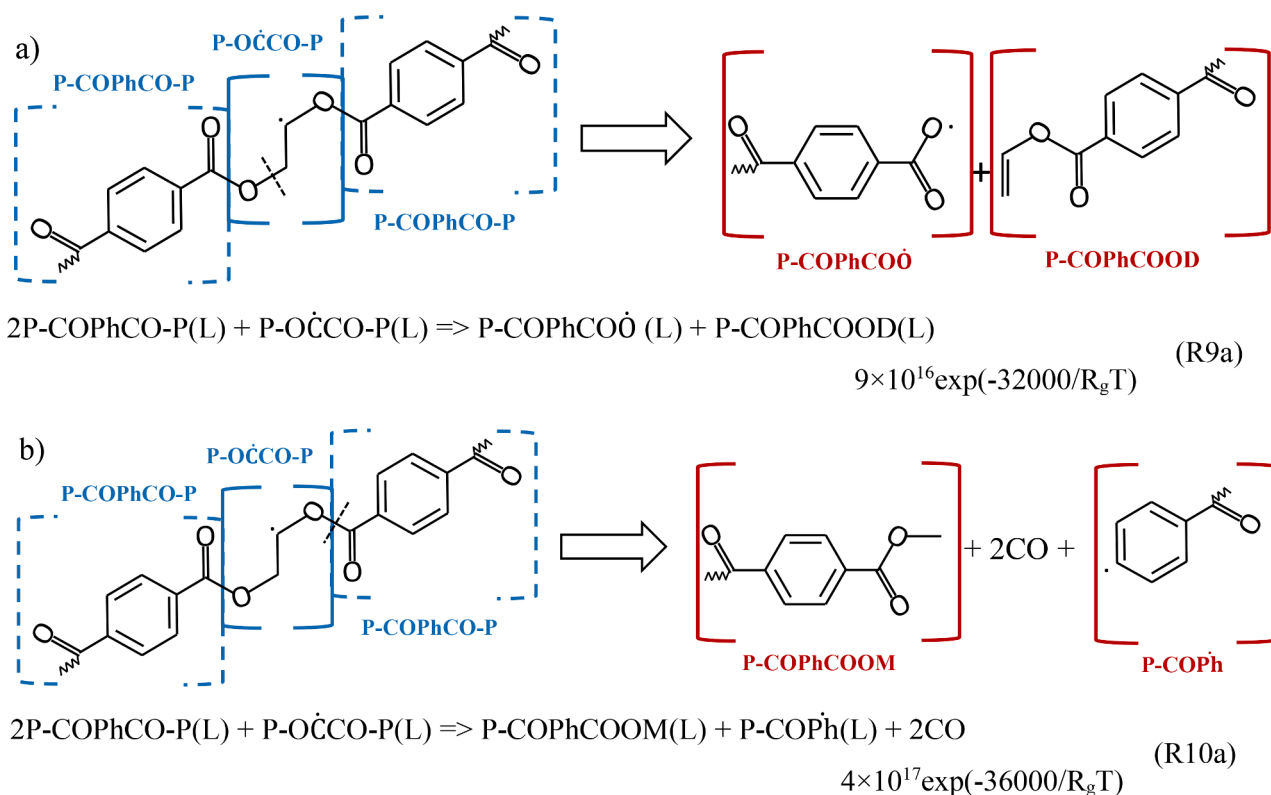


Fig. 4. Representation of the  $\beta$ -scission of the glycol MC radical to form: a) an EC vinyl ester and an EC benzoic radical; b) an EC methyl ester an EC phenyl radical and 2 CO. Species nomenclature employs Ph for  $-\text{C}_6\text{H}_4-$ , C for  $-\text{CH}_2-$ , T for  $-\text{CH}-$ , M for  $-\text{CH}_3$ , and D for  $-\text{C}_2\text{H}_5$ .

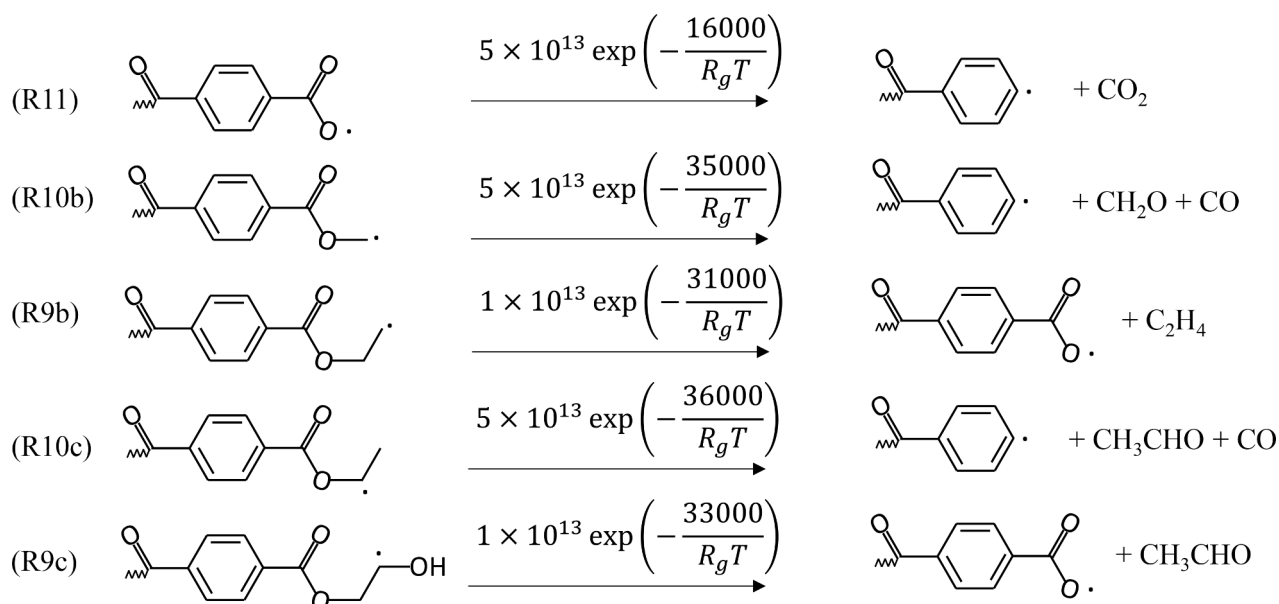


Fig. 5. Schematic representation of the additional beta-scission reactions included in the model.

Arrhenius parameters are similar to other gas-phase acids [100,101] and align closely with the values proposed by Mielczarek et al. [111] and experimentally by Barson and Bevington [112]. The other  $\beta$ -scission reactions involve mainly alkyl-like radicals such as methyl and ethyl esters. The former (R10b) decomposes by breaking the CO-O bond releasing  $\text{CH}_2\text{O}$  and CO, while the latter has two different isomers which decompose according to two different pathways (R9b, R10c). The rate coefficients of these reactions are computed from the elementary classes related to breaking the COO-C (R9) or CO-OC (R10) bonds. The elementary steps are modified to account for the different stabilities of the starting radical. For instance, R10b and R9b employ a decrease of 1 kcal/mol in  $E_{\text{act}}$  due to the lower stability of primary radicals [90,94]. The radical decomposition of glycol end-chains is also considered. The only radical considered is the  $\alpha$ -position to the OH group (P-OC $\dot{\text{C}}$ OH) due to its lower BDE, which decomposes to  $\text{CH}_3\text{CHO}$  and a benzoic radical (R9c). Compared to  $\beta$ -scission of the mid-chain glycol radical (R9a), an increase by 1 kcal/mol in the activation energy is considered due to the higher stability of P-OC $\dot{\text{C}}$ OH.

#### 3.4.4. Glycol 1–5 isomerization

The proposed  $\beta$ -scission parameters lead to an accumulation of glycol radicals. A key pathway proposed herein for glycol radical consumption is the isomerisation by interaction with the ester moiety through a 5-membered ring to form a primary ethylidene diester radical (R12a), as

shown in Fig. 6. The rate parameters for this reaction are computed from the backward reaction (R12b), i.e., an isomerisation from primary to secondary radical. The considered  $E_{\text{act}}$  is similar to 1–4 backbiting (BB 1–4) in PE [53], but a higher frequency factor is considered due to the more rigid C=O bond. The rate parameters of the forward reaction (R12a) are computed from equilibrium considerations. An increase of 4 kcal/mol in  $E_{\text{act}}$  is introduced to account for the BDE differences for primary and secondary hydrogens adjacent to the ester group, as reported by El-Nahas et al. [95]. Additionally, the entropy difference between isobutyl and 2-butyl is considered, resulting in R12b having a frequency factor that is 2 times higher compared to R12a. The model includes  $\beta$ -scission and H-abstraction reactions for both the primary and tertiary ethylidene radicals. The latter is more stable, but it is hindered by the bulky surroundings and involves higher  $E_{\text{act}}$  to decompose. As discussed in Section 3.3, the main decomposition pathway of the ethylidene are concerted ones (Fig. 3), which are major contributors to acetaldehyde formation.

#### 3.4.5. Radical addition reactions

A peculiar aspect of PET degradation reactivity compared to other polymers lies in the presence of benzene rings along the backbone. These functionalities slow polymer decomposition because of their high BDEs [63], but also facilitate the formation of networks of aromatics. At PET degradation temperatures, glycol radicals decompose slowly, while

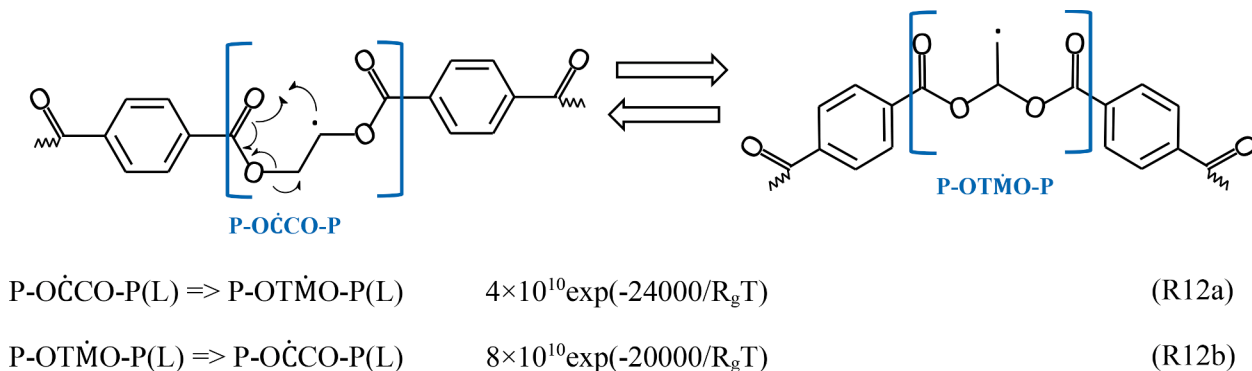


Fig. 6. Schematic representation of isomerisation of the glycol secondary radical to the primary ethylidene position. The backward reaction is considered separately. Species nomenclature employs C for  $-\text{CH}_2-$ , T for  $-\text{CH}-$ , M for  $-\text{CH}_3$ .

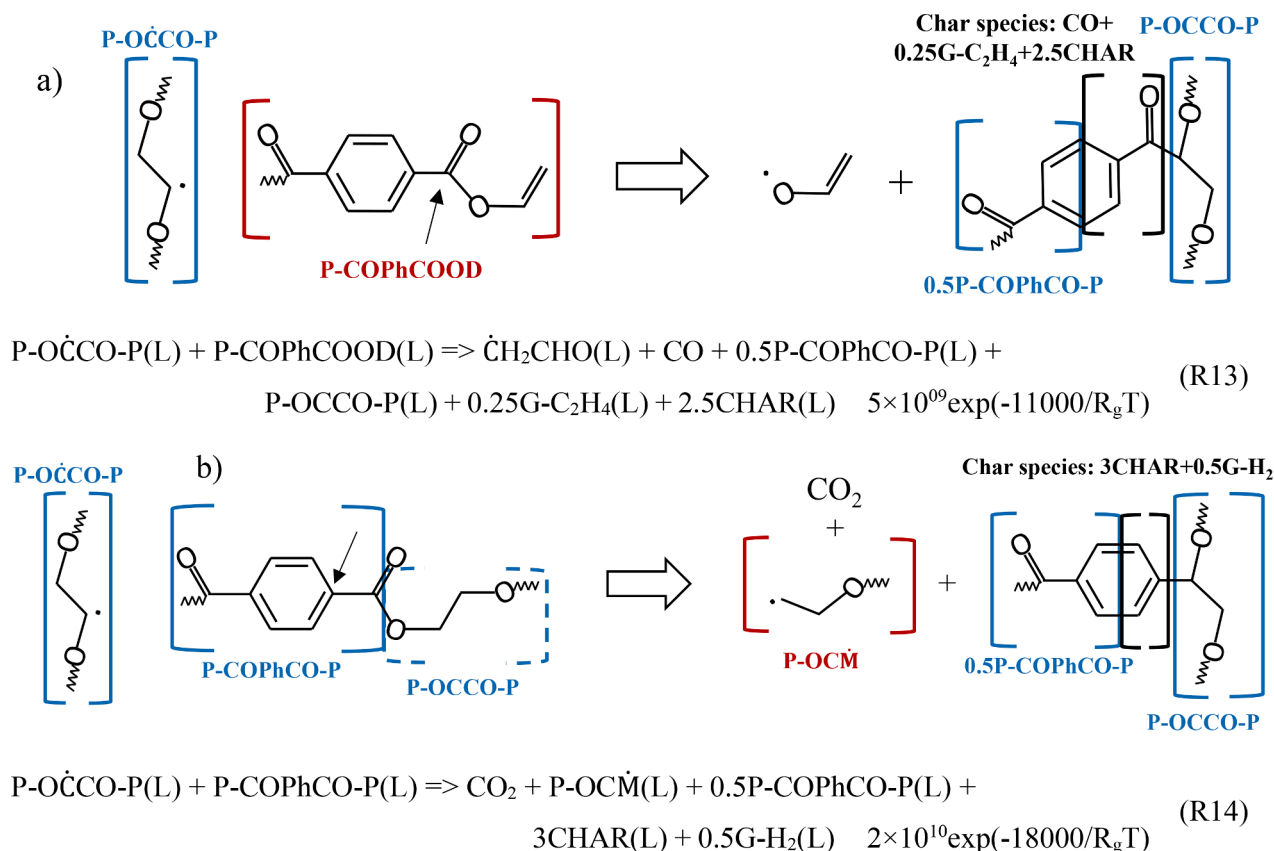


Fig. 7. Schematic representation of glycol radical: a) additions on carbonyl positions of the vinyl ester end-chain; b) aromatic additions on the mid-chain aromatic rings. Species nomenclature employs Ph for  $-\text{C}_6\text{H}_4-$ , C for  $-\text{CH}_2-$ , T for  $-\text{CH}-$ , M for  $-\text{CH}_3$ , and D for  $-\text{C}_2\text{H}_3$ , and r to identify the radical position.

phenyl radicals are unable to decompose at all, and both can interact with the surrounding electrons by H-abstraction or addition reactions. These reaction classes have been studied for gas-phase species [70,113] and are among the main responsible for soot growth [114]. With respect to PET degradation, the high concentration of both radicals and potential addition sites within the polymeric melt increases the relevance of the addition reactions. Several reaction pathways are considered to account for the various addition positions, leading to the formation of stable polycyclic aromatic structures that gradually evolve into char. Because of the lack of quantitative data, the complex unsaturated and branched products of these reactions are lumped in the CHAR species and its pseudo-species analogously to the anhydrides shown in Fig. 3. Only addition of phenyl and glycol radicals to aromatic rings and carbonyl groups of vinyl esters are considered in the present work. These reactions heavily affect char yield and composition.

Fig. 7 schematically represents additions of mid-chain glycol radicals to vinyl esters and aromatic rings respectively. The former are seldom considered in gas-phase mechanisms due to the dominance of unimolecular degradation pathways at high T. Gas-phase studies suggest that addition occurs on the carbon atom side forming short-lived alkoxy radicals [70]. In the context of PET, these addition reactions are sterically hindered by the aromatic rings, but the decomposition of the resulting alkoxy radical is favoured by formation of stable products [70] such as the ethenol radical. For this reason, only additions to the carbonyl groups of vinyl ester are considered because of the significantly low BDE of the  $\text{CO-OC}_2\text{H}_3$  bond.

Fig. 7a schematically represents carbonyl addition of glycol radicals to vinyl esters, where the addition and decomposition reactions are lumped in a single step. This reaction forms an acetaldehyde radical and an acetophenone-like structure. The latter is represented by incorporating a half-terephthalic moiety alongside a mid-chain alkyl group. The

remaining aromatic part is represented through CHAR, ethylene moieties and gas-phase CO. The kinetic parameters are obtained from analogies to gas-phase studies. The frequency factor is the one of the entrance channel, i.e., the addition step, while the energy barrier is related to the decomposition of the alkoxy radical [113], which is the rate determining step. As described by Curran [70], the frequency factor of the carbonyl addition is determined from an equivalent vinyl addition reaction. Considering vinyl esters, the addition of H to styrene [63] is considered as equivalent to the addition of H to the benzaldehyde, which is the smallest gas-phase analogue studied in literature. To account for the higher steric hindrance of glycol radicals, this frequency factor is then adjusted based on the ratio between the addition of isopropyl radicals with respect to that of H on alkyl ketones [70]. Regarding the energy barrier, the model introduces a decrease by 2 kcal/mol compared to formation of  $\text{CH}_3$  from *tert*-butoxy radicals [70]. This reduction is introduced to represent the higher stability of the ethanol product. Similar reactions are considered also for all other alkyl-like radicals on all vinyl ester moieties, dimers included.

Because of the large amounts of mid-chain aromatic rings, aromatic additions of glycol radicals are introduced as shown in Fig. 7b. These reactions form alkyl aromatic moieties and a formyl-alkoxy-like alkyl radical ( $\dot{\text{C}}\text{OOCH}_2-$ ) which is assumed to instantaneously decarboxylate forming an ethyl ester primary radical. The reaction does not introduce the glycol MC as SPU since it balances out as a product. The alkyl aromatic is represented by the ethylene moiety pseudo-species ( $\text{G-C}_2\text{H}_4$ ) and CHAR. The Arrhenius parameters of these reactions are obtained from the analogous gas-phase additions of alkyl radicals to aromatic rings [63,113]. Compared to carbonyl additions, the frequency factor is 4 times higher to represent the lower steric hindrance.

The addition pathway for phenyl radicals mirrors the behaviour of glycol radicals (Fig. 8). Considering additions to the carbonyl group of

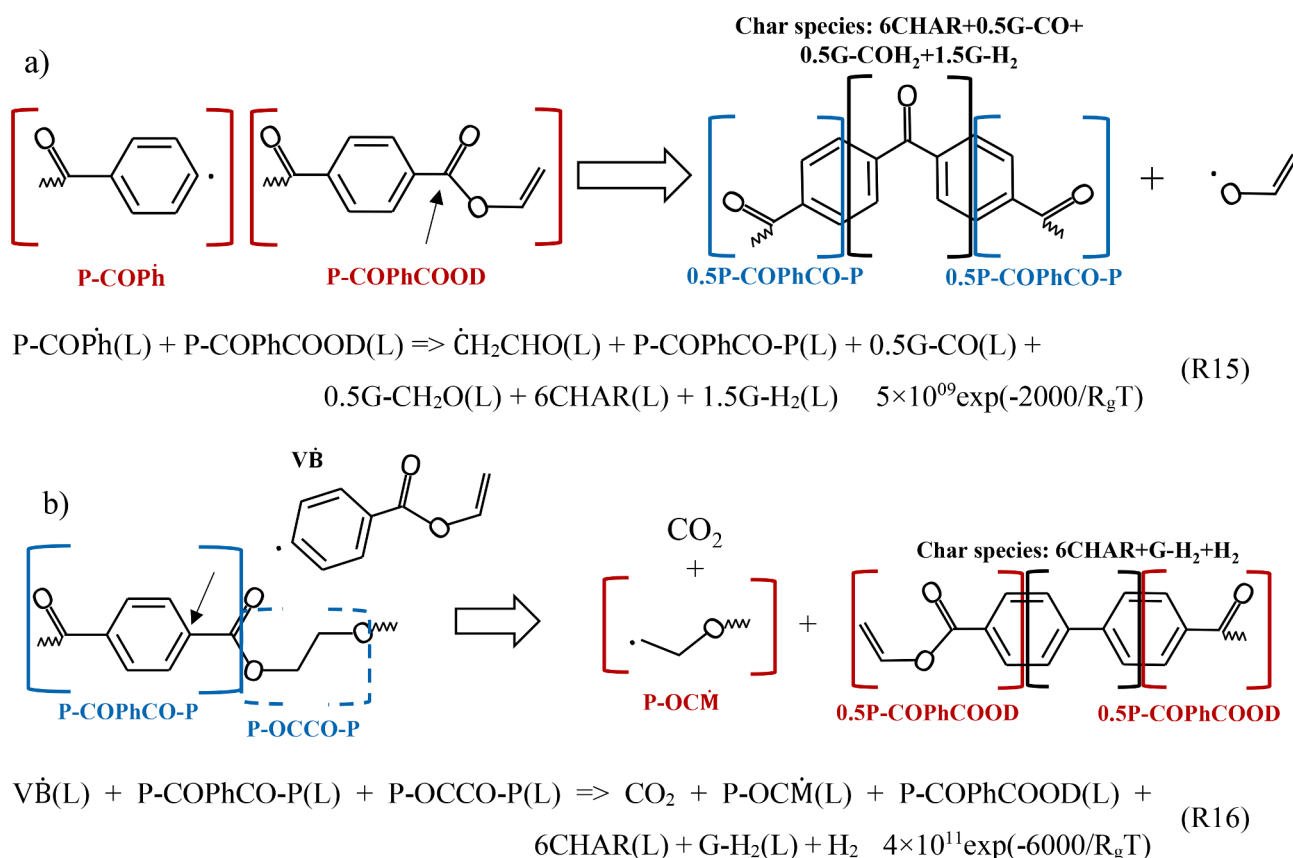


Fig. 8. Schematic representation of: a) phenyl additions to carbonyl groups; b) LMW phenyl radical aromatic additions to mid-chain aromatic rings. Species nomenclature employs Ph for  $-\text{C}_6\text{H}_4-$ , C for  $-\text{CH}_2-$ , T for  $-\text{CH}-$ , M for  $-\text{CH}_3$ , and D for  $-\text{C}_2\text{H}_3$ .

vinyl esters (Fig. 8a), the LMW product remains the same as glycol additions ( $\dot{\text{C}}\text{H}_2\text{CHO}$ ). Conversely, the aromatic structure of the product involves two terephthalic moieties, employing appropriate functional groups to represent the benzophenone-like structure. Three kinds of oxygen and hydrogen pseudo-species describe the variation of carbon content in char with temperature. G-CO and G-CO<sub>2</sub>, respectively, are functional groups bound to the solid residue which release oxygen at intermediate and high T. The latter allows also to account for the hydrogen release at mid-temperature as opposed to the high-temperature release by G-H<sub>2</sub>. The Arrhenius parameters of reaction R15 are obtained by analogy. The same frequency factor that is used for glycol carbonyl addition (R13) is employed here, while the proposed energy barrier is 2 kcal/mol. This value preserves the difference in activation energy between carbonyl addition and H-abstraction of the same radical type. Indeed,  $E_{\text{act}}$  of R15 is 3 kcal/mol lower than the energy barrier of H-abstraction by phenyl radicals (P-COPh) from glycol mid-chains (P-OCCO-P), i.e., 5 kcal/mol [63]. This is the same difference in energy barriers employed for glycol mid-chain radicals comparing H-abstraction and carbonyl addition reactions. Fig. 8b represents addition of the vinyl benzoate phenyl radical to a mid-chain terephthalic moiety (R16). The biphenyl structure involves terephthalic moieties on both sides. These are represented by a vinyl ester end-chain to maintain the radical function of the LMW radical. The remaining structure is described by the CHAR and G-H<sub>2</sub> pseudo-species. Release of H<sub>2</sub> is also included to account for subsequent dehydrogenation of the structure. The reaction is bimolecular but employs a glycol mid-chain as SPU, where the formyloxyl-like radical ( $\dot{\text{C}}\text{OO}-$ ) decarboxylates yielding an ethyl ester radical. With respect to the Arrhenius parameters, the frequency factor is assumed similar to aromatic additions of glycol radicals (R14). On the other hand, the energy barrier proposed is 2 kcal/mol lower than  $E_{\text{act}}$  of C<sub>6</sub>H<sub>5</sub> *ipso*-substitutions of H in soot growth [115–117],

to reflect the 6 kcal/mol lower BDE of Ph-COO groups compared to phenyl hydrogens.

#### 3.4.6. Termination reactions

Only termination by radical–radical recombination (R17) is included in the present mechanism. All combinations of MCs, ECs, and LMW radicals are considered. These reactions lead to an increase in average chain-length, such that the formation of HMW species is represented as a mixture of MC and EC units. These reactions might form highly unsaturated or branched structures, which can lead to char formation. In these cases, to simplify the mechanism, these functionalities are represented as mid-chain and char species. For instance, the recombination of two phenyl end-chain radicals (Fig. S7 of the SM) forms a biphenyl structure as in Fig. 8.b. Recombination reactions are assumed diffusion-controlled [56,76,81,90,94,118,119], and their kinetic parameters are evaluated according to free volume theory [76,81] employing values on viscosity-temperature relations [108] and symmetry considerations in line with polystyrene [120]. As mentioned, the radical pool is assumed being controlled only by HMW species. Since initiation on LMW species is neglected, their termination reactions are not considered to preserve the total radical balance.

## 4. Results

The proposed kinetic model is validated with data from this work and from the previous scientific literature. The comparison involves mass-loss profiles data, volatile distribution, and char characterization. To the best of our knowledge, no other kinetic model is available in the literature for comparison. Setups with negligible transport phenomena and secondary gas-phase reactions (e.g., TG, pyroprobes, micro-pyrolyzers) are considered. Table S10 in the SM reports the data

employed in the present work, the operating conditions, and the source. The observed variability in literature data is attributed to polymer-to-polymer differences and to different experimental setups [7]. For example, Dhahak et al. [17,18] report a  $\sim 10$  °C discrepancy in degradation temperature ( $T_d$ ) between their 2019 and 2020 studies, which differ only by the experimental device employed. More complex models can be employed to account for presence of impurities or transport limitations, but detailed characterization of the material, geometries and flow rates are required. Model performances are evaluated through the Curve Matching (CM) score [121,122]. This approach quantitatively assesses the differences between two curves in terms of point-wise approach and shape dissimilarities, preserving the meaning of the physical trends. In dynamic conditions, a CM score close to unity represents a perfect match, while a score lower than 0.9 corresponds to significant deviations. Conversely, in isothermal conditions a CM of  $\sim 0.9$  represents good agreement. A sensitivity analysis to the reaction mechanism is reported in Section S5 of the SM. The main results of these analyses are discussed in the next Sections.

#### 4.1. Characteristic degradation times

The PET kinetic model is validated with 45 mass-loss profiles from the scientific literature [17–26]. This Section reports only key comparisons, while parity plots and an in-depth analysis of the CM multi-index

approach is reported in Section S4 of the SM. According to the model, the degradation starts from mid-chain syn elimination leading to vinyl and carboxylic end groups (R1a). As degradation proceeds, syn elimination near the end-chains leads to the formation of monomers and dimers with carboxylic and vinyl functionalities (R1b), where the end-chain type dictates the products terminations. Consequently, the molecular mechanism alone results in products with equimolar amounts of carboxylic and vinyl ends, i.e., molar ratios of TA-MVT-DVT of  $\sim 1$ -2-1. This is analogous to the paraffin-olefin-diolefin ratio of PE and PP [76,90,94,123,124]. Among the end-chains molecular pathways, vinyl ester isomerisation is the most significant (R4). This reaction explains the experimentally observed lower abundance of vinyl esters [16] and results in formation of ketene ( $\text{CH}_2\text{CO}$ ) and phenyl ends. Syn elimination (R1) near phenyl end-chains produces vinyl benzoate (VB) and benzoic acid (BA). Formation of vinyl esters initiates the radical mechanism due to the considerably lower BDE which increase the total radical pool (Section 3.4). The radical degradation forms mostly light products and compounds with phenyl ends (e.g., BA). While  $\beta$ -scission of glycol radicals (R9-R10) only proceeds at high T, addition and isomerisation reactions contribute to the low T degradation of carboxylic and vinyl ends. Specifically, radical decarboxylation (R11) and carbonyl additions (R13, R15) result in low quantities of TA and DVT, respectively. Addition reactions are the primary drivers of char formation (R13-R16), also influencing the elemental composition. Char description remains a key

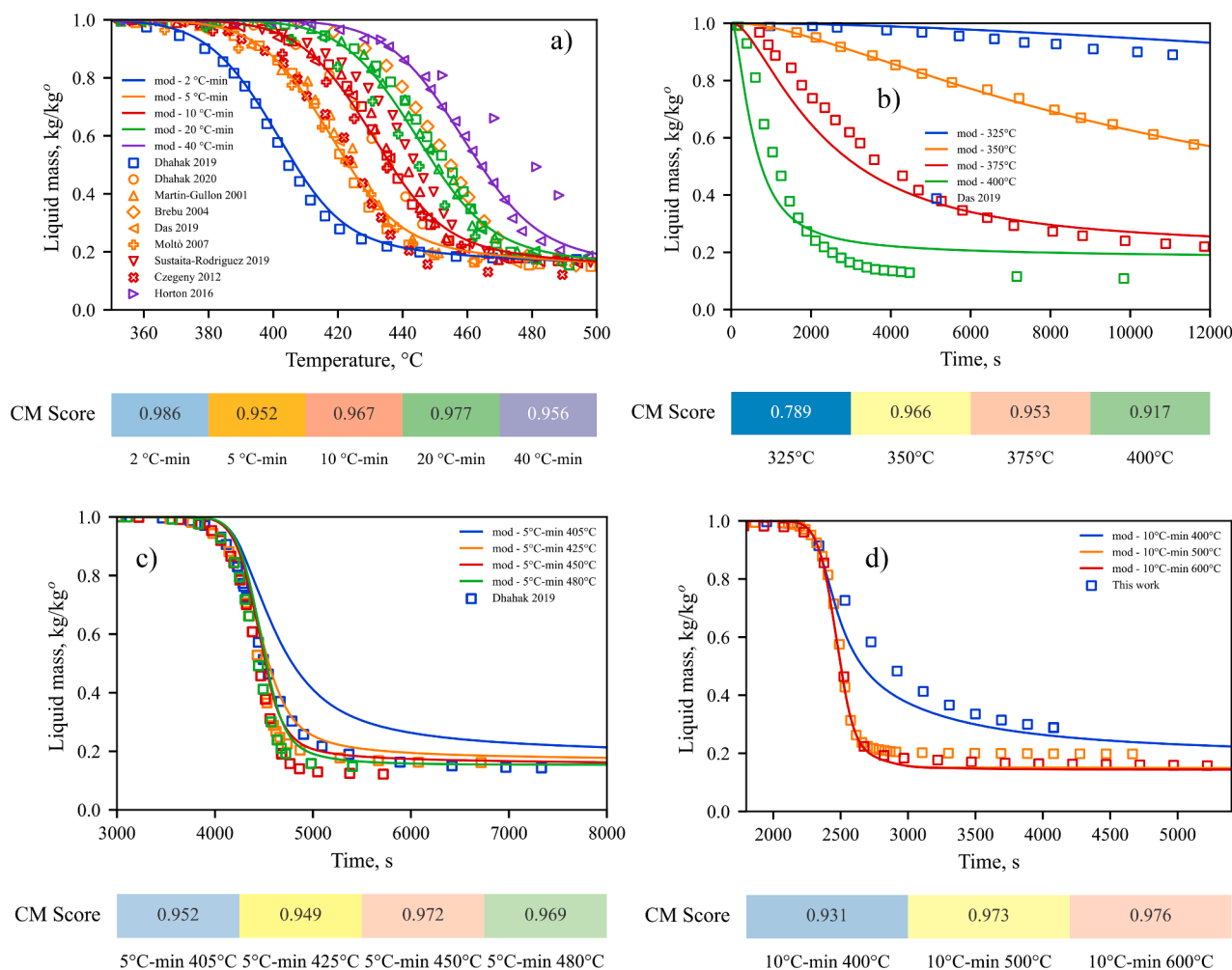


**Fig. 9.** Comparison of predicted (lines) and measured (symbols) mass-loss at: a) HR = 2–40 °C/min [17–24,26], b) T = 325–400 °C [21], c) HR = 5 °C/min and T = 405–480 °C [17], d) HR = 10 °C/min and T = 400–600 °C. The colour identifies the operating conditions, while the marker style the author, e.g., green crosses in a) are data of Moltò et al. (2007) [22] at 20 °C/min. The CM score [122] is reported with the same colour legend as the plot. (For interpretation of the references to colour in this figure legend, the reader is referred to the web version of this article.)

source of uncertainty in the current model. As discussed in Section 3.1, plastic char employs the same species of biochar because of the limited characterization data available for polymer chars. While this framework offers robustness, it is tailored for phenolic and ether moieties that release mainly water and CO. Conversely, PET degradation involves phenone and ester linkages, which are neglected in the species of the biomass mechanism. Nevertheless, since PET is present in low quantities in PW, improvement to this secondary release has a minor impact on the overall product distribution from PW pyrolysis.

As shown in Fig. 9, the model correctly captures the degradation profiles in the entire temperature range. The plots herein reported employ a combination of colour and marker legend to identify the operating conditions (colour) and author (marker). For instance, considering Fig. 9a, which shows the comparison of mass-loss profiles in dynamic conditions, experimental data by Dhahak et al. (2019) [17] are identified by squares. Therefore, the data of Dhahak et al. (2019) at 2 °C/min are identified by blue squares, 5 °C/min by orange squares, 10 °C/min by red squares, and 20 °C/min by green squares. Deviations are usually within a 5 °C range, with some discrepancies reaching up to 50 °C. For instance, at a HR of 5 °C/min, the data from Brebu et al. [20] (orange diamonds) exhibit a  $T_d \sim 40$  °C higher than other studies at 5 °C/min but similar to the  $T_d$  at HR of 20 °C/min. Similarly, at HR of 10 °C/min Czegeny et al. [24] (red crosses) measure a  $T_d \sim 20$  °C lower than others. Significant variations in char yields are also observed (11–20 wt%, see Fig. S12). Generally, higher temperatures lead to lower char amounts and a higher carbon content [55,80,83], but the polymer variability appears more pronounced than the temperature one. For example, Czegeny et al. [24] report a char yield of 11.5 wt% at HR = 10 °C/min and 500 °C, while other authors measure values of  $\sim 16$  wt%. Inorganic impurities might be responsible for these variations [80], but, to the authors' knowledge, no dedicated studies are reported for char formation from PET.

Fig. 9b shows the mass-profiles in isothermal conditions compared to data of Das and Tiwari [21]. At  $T = 325$  °C the model slightly underestimates the polymer reactivity as represented by the low CM score. At  $T = 400$  °C the model overestimates the char yield, predicting 19 wt% at 9000 s compared to the experimental 11 wt%. However, model predictions are consistent with the 15 % value by Das and Tiwari [21] at HR = 5 °C/min (orange left-oriented triangle in Fig. 9a). As the dynamic degradation occurs at  $T > 430$  °C, the model consistently estimates at  $T = 400$  °C a yield higher than HR = 5 °C/min ( $>15$  %). Fig. 9c shows the comparison in quasi-isothermal conditions, heating the sample at HR = 5 °C/min until a constant set temperature. Compared to the data by Dhahak et al. [17], the model underestimates polymer reactivity and overestimates char yields. The non-monotonic decrease in char yield observed by Dhahak et al. [17] might result from experimental uncertainty. Fig. 9d shows the comparison with the experimental investigation performed in this work. The model overestimates the low T reactivity while underestimating the high T char yield, which is the opposite behaviour when compared with the data by Dhahak et al. [17]. This difference is possibly attributed to the experimental variability of the polymer. As shown in Fig. 9a, with HR of 10 °C/min polymer degradation occurs at  $T \sim 460$  °C. For this reason, PET pyrolysis ends before reaching the isothermal plateau of 500 and 600 °C, and both model and experimental curves overlap, except for the char yields. Nevertheless, the model underestimates char formation at 500 °C, although the predicted elemental composition has good agreement with experimental data (see Section 4.3). Developing functional groups specific for PET char is expected to improve model predictions but would require additional data.

#### 4.2. Volatile yields

The degradation products of PET have been investigated in the literature since the 1950s [16,43]. However, quantitative data under kinetically controlled conditions remain scarce [17,27,28]. Product

identification is relevant as it provides insights into the active decomposition reaction pathways, but it does not allow quantitative assessment of the selectivity for model validation purposes. The main volatiles observed in literature are benzoic acid (BA), acetaldehyde, CO, and CO<sub>2</sub>. A key discrepancy exists between predicted and observed amounts of vinyl esters, requiring further investigation.

The model accurately predicts CO<sub>2</sub> yield at both low and high T but underestimates it at intermediate temperatures (500–600 °C). In the present model, the main pathways are decarboxylation of benzoic radicals and additions to mid-chain terephthalic moieties (R12, R14). CO formation is reasonably captured at low and medium temperatures but deviates significantly at  $T = 1000$  °C, likely related to secondary gas-phase reactions. These reactions can result in further decomposition to lighter products (CO, CO<sub>2</sub>) but also formation of heavier aromatic compounds [125]. Defining the complementary gas-phase kinetics is expected to improve model predictions but is outside the scope of the present work. The main responsible for CO formation are addition reactions (R13) and high-temperature  $\beta$ -scissions (R10). With respect to the acetaldehyde yield, the model underestimates its formation at low and medium temperatures but captures its variations. Improving the description of the char yield is expected to also increase the accuracy of CH<sub>3</sub>CHO predictions. Ethylene yield is underestimated by the model, particularly at higher temperatures. The primary pathway involves degradation of end-chain P-OCM species (Fig. 5), which is formed from aromatic additions reactions on terephthalic moieties (R14, R16). However, an increased contribution from this pathway would also lead to overestimation of CO<sub>2</sub> and char.

Fig. 10 shows the volatiles released from PET pyrolysis at different operating conditions. In particular, the comparisons show model predictions and literature experimental results at  $T = 400$ –480 °C [17] (Fig. 10a), this work's experiments at  $T = 400$ –600 °C (Fig. 10b), and literature data at nominal  $T = 700$ –1000 °C [27] (Fig. 10c). As with Fig. 9, data at the same operating conditions share the same colour, while data from the same author share the same bar pattern. The present experimental study finds CO<sub>2</sub>, CH<sub>3</sub>CHO, and benzoic acid being the most abundant products, with low amounts of benzene (2–5 wt%), vinyl benzoate (1–4 wt%), and ethylene (0–4 wt%). Tables S6–S9 in the SM report the detailed experimental results and the lumping of all compounds for comparison with the species tracked in the model. The present observations generally align with literature values [17,27]. However, in this work no CO was detected at 400 °C possibly because of elution through the cryo-trap at long reaction times (25 min), while terephthalic acid (TA) was identified only at 400 °C. The reduction in TA yield at higher temperatures (Fig. 10c) is consequent to radical decarboxylation to BA and C<sub>6</sub>H<sub>6</sub>. The measured VB yields are significantly lower compared to Day et al. [27] ( $\sim 10$  wt%), while Dhahak et al. [17] did not detect it. Compounds such as monovinyl terephthalate (MVT), divinyl terephthalate (DVT), dimers and trimers were not identified. As mentioned, the mass closure is poor at 400 °C, although in line with Dhahak et al. [17]. This is possibly due to high boiling products not detected by the equipment employed [58] (e.g., dimers and trimers) and incomplete polymer conversion. Indeed, TG data show a 29 wt% solid residue 25 min after the set temperature (Fig. 9d). While Day et al. [27] measured significant formation of acetylene, this product might actually correspond to ethylene as measured by Dhahak et al. [17] and in our study. The two compounds have closely overlapping peaks, and the C<sub>2</sub>H<sub>2</sub> found in the present study is not reported as it is in only trace amounts.

The model captures the overall trends in the yields of the main compounds but exhibits some discrepancy. Specifically, the reaction families approach employed intrinsically relates the formation trends of some species opposite to experimental observations. For instance, BA, VB, and CO<sub>2</sub> formation are mechanistically linked through decarboxylation reactions (R11, in Fig. 5) of benzyloxyl radicals, i.e., BA from TA and VB from MVT. BA and VB are also formed from syn elimination (R1)

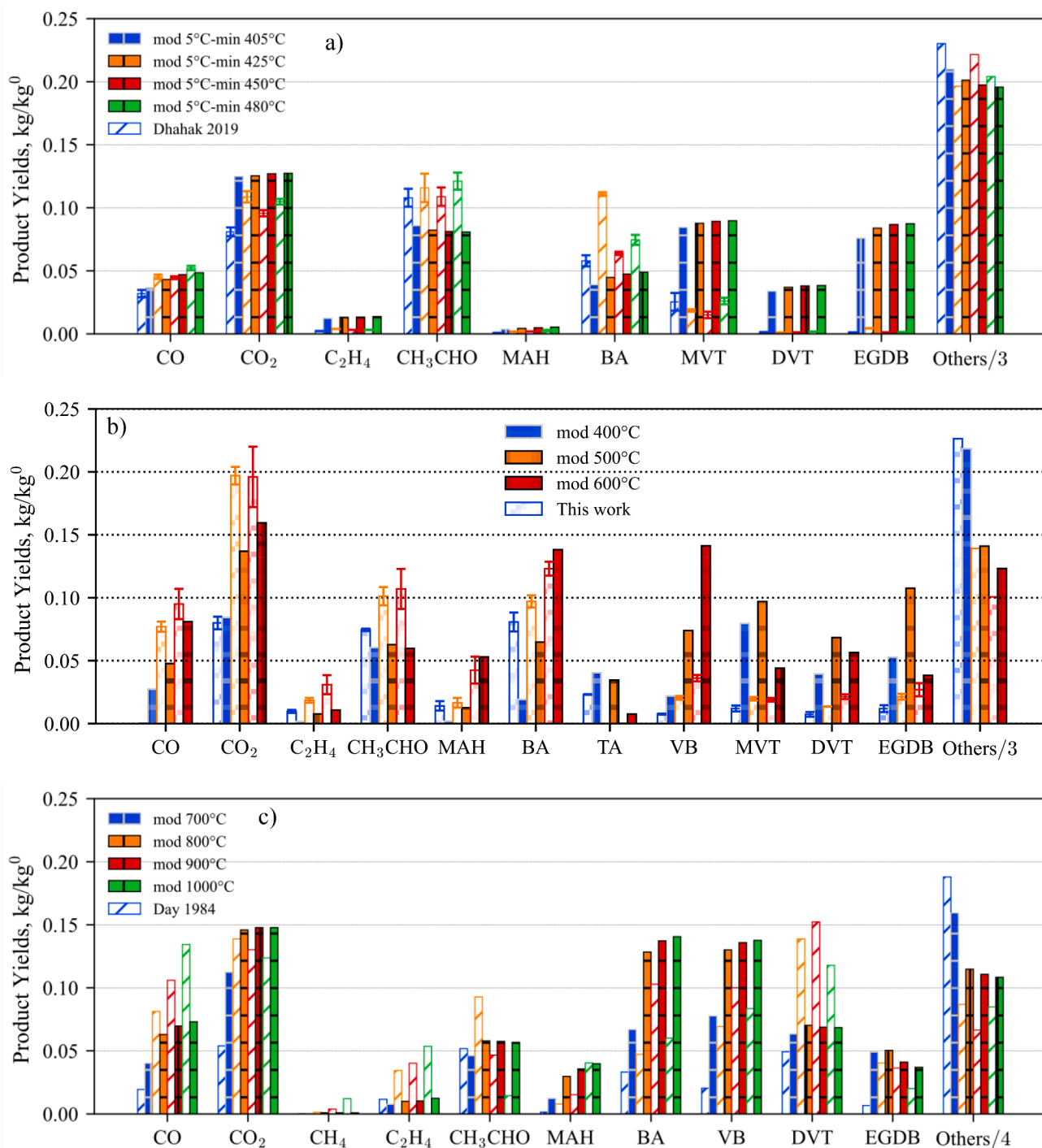


**Fig. 10.** Comparison of measured (patched bars) and predicted (solid bars) volatile yields for: a) low-T pyrolysis in tubular reactors [17], b) medium T in the micropyrolyzer employed in this work, c) high T in a pyroprobe [27]. The species names are the same employed in the model, except for MAH which stands for monocyclic aromatic hydrocarbons (e.g., benzene, toluene).

near phenyl end-chains (P-COPhH), which forms ethylene glycol dibenzoate (EGDB) as well. The latter also accounts for dimers with 1 phenyl termination by horizontal lumping [125]. Since BA, VB, and EGDB are inherently related, the model predicts similar molar yields. Preferential dimer degradation pathways are responsible for the low yields of EGDB at high temperature, but the low experimental yields of VB are possibly related to the polymerization of vinyl bonds similarly to diolefins in PE, PP, and PS [76]. Similarly, CH<sub>3</sub>CHO and char yields are intertwined. The model predicts acetaldehyde formation from reactions leading to aromatic precursors such as carbonyl additions (R13, R15)

and ethylidene degradation (R1c).

With respect to higher molecular weight compounds, more discrepancies are observed even among different experimental data sets. As mentioned, the model predicts comparable amounts of vinyl and carboxylic end groups, while significant vinyl ester formation is only observed by Day et al. [27] at high T. The model underestimates the DVT yield of Day et al. [27], but the combination of MVT and DVT is consistent with the experimental measurements. As previously mentioned, both acids and vinyl esters derive from mid-chain degradations, either from glycol radical  $\beta$ -scissions (R9) or syn elimination



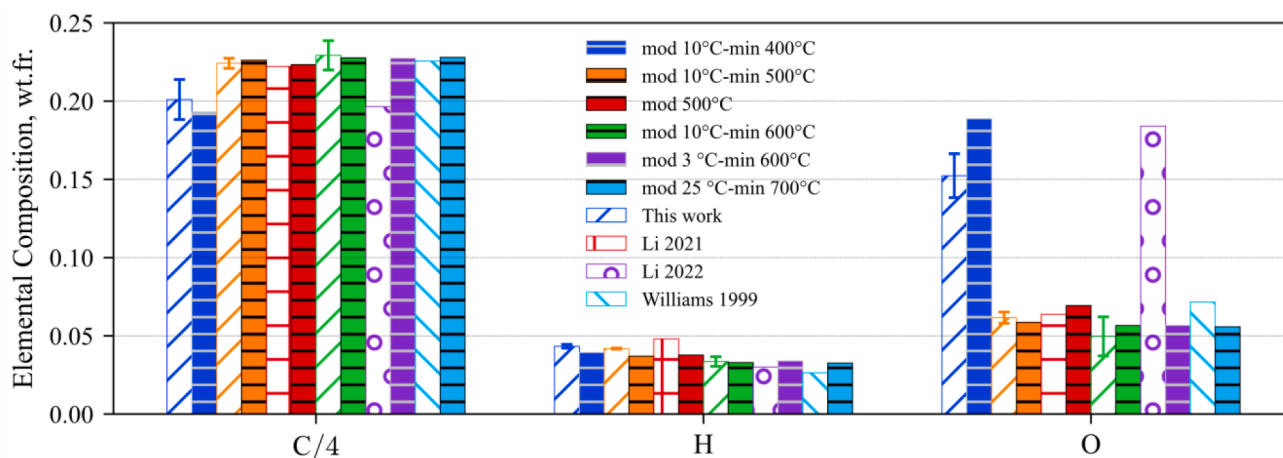


Fig. 11. Comparison of char elemental composition for the present model (solid bars) and both literature [29–31] and new experimental data (patched bars).

pathways (R1). Overall, the model predicts lower amounts of carboxylic ends than vinyl esters, consistently with the high-temperature data by Day et al. [27]. Conversely, it overestimates MVT yield compared to data of Dhahak et al. [17] (1–4 wt%), who detected neither DVT nor vinyl benzoate. Similarly, in the present experimental campaign only low amounts of VB and DVT were found (1–3 wt%) and no MVT was identified. As mentioned, the model predicts amounts of VB, MVT, and DVT of 3–15, 15, and 3–7 wt%, respectively. Degradation of vinyl esters (R4) decreases their yields increasing benzene formation, which is already overestimated by the model because of these pathways. Further experimental and modelling work is required to better assess the reactivity of vinyl esters.

#### 4.3. Char characterization

Fig. 11 shows the comparison between experimental measurements and model prediction with respect to char elemental composition. As with Fig. 9, data at the same operating conditions share the same colour, while data from the same author share the same bar pattern. In general, increasing the temperature is expected to produce solid residues with high carbon content, while low temperature pyrolysis results in higher oxygen content. Experimental data show that plastic char has a higher H content than the initial polymer, while most of the oxygen is lost upon pyrolysis [29–31]. The model correctly reproduces these trends and shows good agreement with the present char characterization data and values by Li et al. (2021) [31]. Conversely, deviations are observed with the data by Li et al. (2022) [29] and Williams and Williams [30]. The predicted higher C% results from the severe operating conditions. While low and medium heating rates are employed for the pyrolysis, the authors report heating the samples to 600 and 700 °C respectively, which according to the model results in high C% and low O%. The model predictions are in line with the other data shown in Fig. 11 which have lower final temperatures.

## 5. Conclusions

The present work proposes a condensed-phase semi-detailed kinetic model for thermal degradation of PET coupled with new experimental investigations. To the best of the authors' knowledge, this is the first quantitative kinetic mechanism for PET pyrolysis.

Following the functional groups methodology, the model describes polymeric chains through pseudo-species representative of the chemical moieties, while short compounds of interest are represented in greater detail. Because of the lack of experimental data, the PET char is modelled through the same framework of biochar formation during biomass pyrolysis. The kinetic mechanism incorporates both molecular

and radical pathways and is developed through a first-principle approach. Reactions proposed in the scientific literature are critically assessed, employing kinetic parameters obtained from analogous gas-phase compounds through a reaction class-based approach. Further work will address estimation through theoretical methodologies of the condensed-phase rate constants [77].

The model is validated considering new data as well as literature data in terms of mass profiles, volatile yields, and char characterization. The model accurately predicts mass loss profiles, although there is significant variability in experimental char yield data that the model obviously cannot fully capture. Regarding volatile products, the model captures the trends observed for the major components. However, it overestimates the vinyl ester to acid ratio compared to some experimental observations, likely due to similar reaction pathways described in the model for both products. Further experimental work is required to investigate and quantify the heavy pyrolysis products (e.g., dimers) to reach reasonable mass closures also at 400 °C. The model proves capable to describe also char elemental composition, but a broader experimental validation range is required.

The proposed mechanism is provided in CHEMKIN format as SM and it is freely accessible on GitHub [79]. The model specifically addresses condensed-phase reactivity, and future work will extend its application to assess gasification reactivity. The present investigation constitutes a key step towards modelling the chemical recycle of plastic waste mixtures. Future experimental and modelling work will address interactions of PET, PVC, and PA.

#### CRediT authorship contribution statement

**A. Locaspi:** Writing – original draft, Visualization, Validation, Methodology, Investigation, Formal analysis, Data curation, Conceptualization. **O. Akin:** Writing – review & editing, Investigation. **D. Withoek:** Writing – review & editing, Investigation. **M. Havaei:** Writing – review & editing, Investigation. **A. Frassoldati:** Writing – review & editing, Methodology, Formal analysis. **L. Pratali Maffei:** Writing – review & editing, Methodology, Investigation. **M. Pelucchi:** Writing – review & editing, Methodology. **M. Mehl:** Methodology, Investigation. **R.J. Varghese:** Writing – review & editing, Supervision, Data curation. **K.M. Van Geem:** Writing – review & editing, Supervision, Resources, Funding acquisition. **T. Faravelli:** Writing – review & editing, Supervision, Resources, Project administration, Funding acquisition, Conceptualization.

#### Declaration of competing interest

The authors declare the following financial interests/personal

relationships which may be considered as potential competing interests: Tiziano Faravelli reports financial support was provided by European Commission. Kevin Van Geem reports financial support was provided by European Research Council. If there are other authors, they declare that they have no known competing financial interests or personal relationships that could have appeared to influence the work reported in this paper.

## Acknowledgments

This project has received funding from the European Union's Horizon Europe research and innovation programme under the HORIZON-CL4-2021-TWIN-TRANSITION-01 grant agreement No 101058412. Views and opinions expressed are however those of the author(s) only and do not necessarily reflect those of the European Union or HADEA. Neither the European Union nor the granting authority can be held responsible for them. UGENT acknowledges funding from the European Research Council under the European Union's Horizon 2020 research and innovation programme/ERC grant agreement n° 818607.

## Appendix A. Supplementary data

Supplementary data to this article can be found online at <https://doi.org/10.1016/j.cej.2024.156955>.

## Data availability

Data will be made available on request.

## References

- [1] A.R. Rahimi, J.M. Garcíá, Chemical recycling of waste plastics for new materials production, *Nat. Rev. Chem.* 16 (1) (2017) 1–11, <https://doi.org/10.1038/s41570-017-0046>.
- [2] W. Kaminsky, Chemical recycling of mixed plastics of pyrolysis, *Adv. Polym. Tech.* 14 (1995) 337–344, <https://doi.org/10.1002/ADV.1995.060140407>.
- [3] K.M. Van Geem, Plastic waste recycling is gaining momentum, *Science* (80-) 381 (2023) 607–608, <https://doi.org/10.1126/science.adj2807>.
- [4] K. Ragaert, L. Delva, K. Van Geem, Mechanical and chemical recycling of solid plastic waste, *Waste Manag.* 69 (2017) 24–58, <https://doi.org/10.1016/j.wasman.2017.07.044>.
- [5] L. Brivio, F. Tollini, PET recycling: review of the current available technologies and industrial perspectives, in: *Adv. Chem. Eng., Academic Press*, 2022, pp. 215–267, <https://doi.org/10.1016/bs.ache.2022.09.003>.
- [6] U. Arena, Process and technological aspects of municipal solid waste gasification. A review, *Waste Manag.* 32 (2012) 625–639, <https://doi.org/10.1016/j.wasman.2011.09.025>.
- [7] O. Dogu, M. Pelucchi, R. Van de Vijver, P.H.M. Van Steenberghe, D.R. D'hooge, A. Cuoci, M. Mehl, A. Frassoldati, T. Faravelli, K.M. Van Geem, The chemistry of chemical recycling of solid plastic waste via pyrolysis and gasification: state-of-the-art, challenges, and future directions, *Prog. Energy Combust. Sci.* 84 (2021) 100901, <https://doi.org/10.1016/j.pecs.2020.100901>.
- [8] A. López, I. de Marco, B.M. Caballero, M.F. Laresgoiti, A. Adrados, Pyrolysis of municipal plastic wastes: Influence of raw material composition, *Waste Manag.* 30 (2010) 620–627, <https://doi.org/10.1016/j.wasman.2009.10.014>.
- [9] M.S. Talmadge, R.M. Baldwin, M.J. Bidy, R.L. McCormick, G.T. Beckham, G. A. Ferguson, S. Czernik, K.A. Magrini-Bair, T.D. Foust, P.D. Metelski, C. Hetrick, M.R. Nimlos, A perspective on oxygenated species in the refinery integration of pyrolysis oil, *Green Chem.* 16 (2014) 407–453, <https://doi.org/10.1039/C3GC41951G>.
- [10] L. Goulet, R.E. Prud'Homme, Dégradation thermique de mélanges miscibles et immiscibles polyester/polychlorure de vinyle, *Eur. Polym. J.* 22 (1986) 529–536, [https://doi.org/10.1016/0014-3057\(86\)90179-5](https://doi.org/10.1016/0014-3057(86)90179-5).
- [11] I. Coralli, V. Giorgi, I. Vassura, A.G. Rombolà, D. Fabbri, Secondary reactions in the analysis of microplastics by analytical pyrolysis, *J. Anal. Appl. Pyrol.* 161 (2022) 105377, <https://doi.org/10.1016/j.jaap.2021.105377>.
- [12] B. Li, X. Wang, Z. Xia, W. Zhou, Y. Wu, G. Zhu, Co-pyrolysis of waste polyester enameled wires and polyvinyl chloride: evolved products and pyrolysis mechanism analysis, *J. Anal. Appl. Pyrol.* 169 (2023) 105816, <https://doi.org/10.1016/j.jaap.2022.105816>.
- [13] R. Knümann, H. Bockhorn, Investigation of the kinetics of pyrolysis of PVC by TG-MS-analysis, *Combust. Sci. Technol.* 101 (1994) 285–299, <https://doi.org/10.1080/00102209408951877>.
- [14] B.A. Perez, J.V. Jayarama Krishna, H.E. Toraman, Insights into co-pyrolysis of polyethylene terephthalate and polyamide 6 mixture through experiments, kinetic modeling and machine learning, *Chem. Eng. J.* 468 (2023) 143637, <https://doi.org/10.1016/j.cej.2023.143637>.
- [15] S. Madanikashani, L.A. Vandewalle, S. De Meester, J. De Wilde, K.M. Van Geem, Multi-scale modeling of plastic waste gasification: opportunities and challenges, *Materials* (Basel) 15 (2022) 4215, <https://doi.org/10.3390/ma15124215>.
- [16] R.J.P. Allan, A Study of the Pyrolysis of Poly(Ethylene Terephthalate) by means of Model Systems, University of Glasgow, 1956.
- [17] A. Dhahak, G. Hild, M. Rouaud, G. Mauviel, V. Burkle-Vitzthum, Slow pyrolysis of polyethylene terephthalate: online monitoring of gas production and quantitative analysis of waxy products, *J. Anal. Appl. Pyrol.* 142 (2019) 104664, <https://doi.org/10.1016/j.jaap.2019.104664>.
- [18] A. Dhahak, C. Grimmer, A. Neumann, C. Rüger, M. Sklorz, T. Streibel, R. Zimmermann, G. Mauviel, V. Burkle-Vitzthum, Real time monitoring of slow pyrolysis of polyethylene terephthalate (PET) by different mass spectrometric techniques, *Waste Manag.* 106 (2020) 226–239, <https://doi.org/10.1016/j.wasman.2020.03.028>.
- [19] I. Martín-Gullón, M. Esperanza, R. Font, Kinetic model for the pyrolysis and combustion of poly-(ethylene terephthalate) (PET), *J. Anal. Appl. Pyrol.* 58–59 (2001) 635–650, [https://doi.org/10.1016/S0165-2370\(00\)00141-8](https://doi.org/10.1016/S0165-2370(00)00141-8).
- [20] M. Brebu, T. Bhaskar, K. Murai, A. Muto, Y. Sakata, M.A. Uddin, The effect of PVC and/or PET on thermal degradation of polymer mixtures containing brominated ABS, *Fuel* 83 (2004) 2021–2028, <https://doi.org/10.1016/j.fuel.2004.04.011>.
- [21] P. Das, P. Tiwari, Thermal degradation study of waste polyethylene terephthalate (PET) under inert and oxidative environments, *Thermochim. Acta* 679 (2019) 178340, <https://doi.org/10.1016/j.tca.2019.178340>.
- [22] J. Moltó, R. Font, J.A. Conesa, Kinetic model of the decomposition of a PET fibre cloth in an inert and air environment, *J. Anal. Appl. Pyrol.* 79 (2007) 289–296, <https://doi.org/10.1016/j.jaap.2006.12.006>.
- [23] J.M. Sustaita-Rodríguez, F.J. Medellín-Rodríguez, D.C. Olvera-Mendez, A. J. Gimenez, G. Luna-Barcenas, Thermal stability and early degradation mechanisms of high-density polyethylene, polyamide 6 (nylon 6), and polyethylene terephthalate, *Polym. Eng. Sci.* 59 (2019) 2016–2023, <https://doi.org/10.1002/PEN.25201>.
- [24] Z. Czégény, E. Jakab, M. Blazsó, T. Bhaskar, Y. Sakata, Thermal decomposition of polymer mixtures of PVC, PET and ABS containing brominated flame retardant: formation of chlorinated and brominated organic compounds, *J. Anal. Appl. Pyrol.* 96 (2012) 69–77, <https://doi.org/10.1016/j.jaap.2012.03.006>.
- [25] A. Brems, J. Baeyens, J. Beerlandt, R. Dewil, Thermogravimetric pyrolysis of waste polyethylene-terephthalate and polystyrene: a critical assessment of kinetics modelling, *Resour. Conserv. Recycl.* 55 (2011) 772–781, <https://doi.org/10.1016/j.resconrec.2011.03.003>.
- [26] S.R. Horton, J. Woeckner, R. Mohr, Y. Zhang, F. Petrocchi, M.T. Klein, Molecular-level kinetic modeling of the gasification of common plastics, *Energy Fuel* 30 (2016) 1662–1674, <https://doi.org/10.1021/acs.energyfuels.5b02047>.
- [27] M. Day, D.M. Wiles, Influence of temperature and environment on the thermal decomposition of poly(ethylene terephthalate) fibres with and without the flame retardant tris(2,3-dibromopropyl) phosphate, *J. Anal. Appl. Pyrol.* 7 (1984) 65–82, [https://doi.org/10.1016/0165-2370\(84\)80041-8](https://doi.org/10.1016/0165-2370(84)80041-8).
- [28] S. Du, J.A. Valla, R.S. Parnas, G.M. Bolas, Conversion of polyethylene terephthalate based waste carpet to benzene-rich oils through thermal, catalytic, and catalytic steam pyrolysis, *ACS Sustain. Chem. Eng.* 4 (2016) 2852–2860, <https://doi.org/10.1021/acssuschemeng.6b00450>.
- [29] C. Li, Y. Sun, Q. Li, L. Zhang, S. Zhang, H. Wang, G. Hu, X. Hu, Effects of volatiles on properties of char during sequential pyrolysis of PET and cellulose, *Renew. Energy* 189 (2022) 139–151, <https://doi.org/10.1016/j.renene.2022.02.091>.
- [30] E.A. Williams, P.T. Williams, The pyrolysis of individual plastics and a plastic mixture in a fixed bed reactor, *J. Chem. Technol. Biotechnol.* 70 (1997) 9–20, [https://doi.org/10.1002/\(SICI\)1097-4660\(199709\)70:1<9::AID-JCTB700>3.0.CO;2-E](https://doi.org/10.1002/(SICI)1097-4660(199709)70:1<9::AID-JCTB700>3.0.CO;2-E).
- [31] C. Li, F. Atefi, F. Atashi, X. Hu, M. Gholizadeh, Catalytic pyrolysis of polyethylene terephthalate over zeolite catalyst: characteristics of coke and the products, *Int. J. Energy Res.* 45 (2021) 19028–19042, <https://doi.org/10.1002/ER.7078>.
- [32] D.J. Carlsson, M. Day, T. Suprunchuk, D.M. Wiles, Pyrolysis of poly(ethylene terephthalate) fibers: characterization of involatile residues, *J. Appl. Polym. Sci.* 28 (1983) 715–724, <https://doi.org/10.1002/APP.1983.070280226>.
- [33] G. Montaudo, C. Puglisi, F. Samperi, Primary thermal degradation mechanisms of PET and PBT, *Polym. Degrad. Stab.* 42 (1993) 13–28, [https://doi.org/10.1016/0141-3910\(93\)90021-A](https://doi.org/10.1016/0141-3910(93)90021-A).
- [34] J. Huang, H. Meng, X. Luo, X. Mu, W. Xu, L. Jin, B. Lai, Insights into the thermal degradation mechanisms of polyethylene terephthalate dimer using DFT method, *Chemosphere* 291 (2022) 133112, <https://doi.org/10.1016/j.chemosphere.2021.133112>.
- [35] M. Dröschner, F. Georg Schmidt, The kinetics of the ester-interchange reaction of poly(ethylene terephthalate), *Polym. Bull.* 4 (1981) 261–266, <https://doi.org/10.1007/BF00256315>.
- [36] M.E. Bednas, M. Day, K. Ho, R. Sander, D.M. Wiles, Combustion and pyrolysis of poly(ethylene terephthalate). I. The role of flame retardants on products of pyrolysis, *J. Appl. Polym. Sci.* 26 (1981) 277–289, <https://doi.org/10.1002/APP.1981.070260126>.
- [37] K. Ravindranath, R.A. Mashelkar, Polyethylene terephthalate—I. Chemistry, thermodynamics and transport properties, *Chem. Eng. Sci.* 41 (1986) 2197–2214, [https://doi.org/10.1016/0009-2509\(86\)85070-9](https://doi.org/10.1016/0009-2509(86)85070-9).
- [38] S. Venkatachalam, S.G. Nayak, J.V. Labde, P.R. Gharal, K. Rao, A.K. Kelkar, S. Venkatachalam, S.G. Nayak, J.V. Labde, P.R. Gharal, K. Rao, A.K. Kelkar, Degradation and recyclability of poly(ethylene terephthalate), Polyester. (2012), <https://doi.org/10.5772/48612>.
- [39] D.M. Rhee, W.S. Ha, J.H. Youk, D. Il Yoo, Interchange reaction kinetics and sequence distribution of liquid crystalline poly(ethylene terephthalate-co-2(3)-

- chloro-1,4-phenylene terephthalate), *Fibers Polym.* 22 (2) (2001) 86–91, <https://doi.org/10.1007/BF02875264>.
- [40] E. Leng, M. Costa, Y. Peng, Y. Zhang, X. Gong, A. Zheng, Y. Huang, M. Xu, Role of different chain end types in pyrolysis of glucose-based anhydro-sugars and oligosaccharides, *Fuel* 234 (2018) 738–745, <https://doi.org/10.1016/j.fuel.2018.07.075>.
- [41] B.J. Holland, J.N. Hay, The thermal degradation of PET and analogous polyesters measured by thermal analysis–Fourier transform infrared spectroscopy, *Polymer (Guildf)* 43 (2002) 1835–1847, [https://doi.org/10.1016/S0032-3861\(01\)00775-3](https://doi.org/10.1016/S0032-3861(01)00775-3).
- [42] T. Ma, R. Wang, W. Wang, W. Gu, Y. Yuan, A. Zhang, J. Wei, Studies on the thermal degradation mechanism of polyethylene terephthalate and its 2-carboxy ethyl (phenyl) phosphinic acid copolymers, *Polym. Degrad. Stab.* 206 (2022) 110185, <https://doi.org/10.1016/J.POLYMEDEGRADSTAB.2022.110185>.
- [43] R.L. Adelman, The interchange reaction of vinyl acetate with organic acids, *J. Org. Chem.* 14 (1949) 1057–1077, <https://doi.org/10.1021/jo01158a015>.
- [44] R.J.P. Allan, R.L. Forman, P.D. Ritchie, Studies in pyrolysis. Part IV. Model systems for the pyrolysis of poly(ethylene terephthalate) and allied polyesters, *J. Chem. Soc. (1955)* 2717, <https://doi.org/10.1039/jr9550002717>.
- [45] R.J.P. Allan, E. Jones, P.D. Ritchie, 104. Studies in pyrolysis. Part VIII. Competitive routes in the pyrolysis of esters: alkylene and alkylidene dibenzoates and some related substances, *J. Chem. Soc. (1957)* 524–531, <https://doi.org/10.1039/JR9570000524>.
- [46] L.H. Buxbaum, The degradation of poly(ethylene terephthalate), *Angew. Chem. Int. Ed. Engl.* 7 (1968) 182–190, <https://doi.org/10.1002/ANIE.196801821>.
- [47] G.W. Halek, Zero-order kinetics of acetaldehyde thermal generation from polyethylene terephthalate, *J. Polym. Sci. Part C: Polym. Symp.* (1986) 83–92, <https://doi.org/10.1002/polc.5070740110>.
- [48] A. Locaspi, M. Ferri, F. Serse, M. Maestri, M. Pelucchi, Chemical kinetics of catalytic/non-catalytic pyrolysis and gasification of solid plastic wastes, Academic Press (2022), <https://doi.org/10.1016/BS.ACHE.2022.09.002>.
- [49] S.A. Jenekhe, J.W. Lin, B. Sun, Kinetics of the thermal degradation of polyethylene terephthalate, *Thermochim. Acta* 61 (1983) 287–299, [https://doi.org/10.1016/0040-6031\(83\)80283-4](https://doi.org/10.1016/0040-6031(83)80283-4).
- [50] K.H. Ko, A. Rawal, V. Sahajwalla, Analysis of thermal degradation kinetics and carbon structure changes of co-pyrolysis between macadamia nut shell and PET using thermogravimetric analysis and <sup>13</sup>C solid state nuclear magnetic resonance, *Energy Convers. Manag.* 86 (2014) 154–164, <https://doi.org/10.1016/J.ENCONMAN.2014.04.060>.
- [51] G. Özsin, M. Kılıç, E. Apaydin-Varol, A.E. Pütün, E. Pütün, A thermo-kinetic study on co-pyrolysis of oil shale and polyethylene terephthalate using TGA/FT-IR, *Korean J. Chem. Eng.* 37 (2020) 1888–1898, <https://doi.org/10.1007/s11814-020-0614-2>.
- [52] R.W.J. Westerhout, J. Waanders, J.A.M. Kuipers, W.P.M. Van Swaaij, Kinetics of the low-temperature pyrolysis of polyethylene, polypropylene, and polystyrene modeling, experimental determination, and comparison with literature models and data, *Ind. Eng. Chem. Res.* 36 (1997) 1955–1964, <https://doi.org/10.1021/IE960501M>.
- [53] A. Locaspi, A. Frassoldati, T. Faravelli, Reduced-order condensed-phase kinetic models for polyethylene, polypropylene and polystyrene thermochemical recycling, *Chem. Eng. J.* (2024) 156949, <https://doi.org/10.1016/j.cej.2024.156949>.
- [54] A. Marongiu, T. Faravelli, G. Bozzano, M. Dente, E. Ranzi, Thermal degradation of poly(vinyl chloride), *J. Anal. Appl. Pyrol.* 70 (2003) 519–553, [https://doi.org/10.1016/S0165-2370\(03\)00024-X](https://doi.org/10.1016/S0165-2370(03)00024-X).
- [55] P. Debiagi, G. Gentile, A. Cuoci, A. Frassoldati, E. Ranzi, T. Faravelli, A predictive model of biochar formation and characterization, *J. Anal. Appl. Pyrol.* 134 (2018) 326–335, <https://doi.org/10.1016/J.JAAP.2018.06.022>.
- [56] A. Locaspi, M. Pelucchi, T. Faravelli, Towards a lumped approach for solid plastic waste gasification: polystyrene pyrolysis, *J. Anal. Appl. Pyrol.* 171 (2023) 105960, <https://doi.org/10.1016/J.JAAP.2023.105960>.
- [57] Y. Ureeł, M.R. Dobbelaere, O. Akin, R.J. Varghese, C.G. Pernalet, J.W. Thybaut, K.M. Van Geem, Active learning-based exploration of the catalytic pyrolysis of plastic waste, *Fuel* 328 (2022) 125340, <https://doi.org/10.1016/J.FUEL.2022.125340>.
- [58] A. Eschenbacher, R.J. Varghese, E. Delikonstantis, O. Mynko, F. Goodarzi, K. Enemark-Rasmussen, J. Oenema, M.S. Abbas-Abadi, G.D. Stefanidis, K.M. Van Geem, Highly selective conversion of mixed polyolefins to valuable base chemicals using phosphorus-modified and steam-treated mesoporous HZSM-5 zeolite with minimal carbon footprint, *Appl. Catal. B Environ.* 309 (2022) 121251, <https://doi.org/10.1016/J.APCATB.2022.121251>.
- [59] A. Eschenbacher, R.J. Varghese, J. Weng, K.M. Van Geem, Fast pyrolysis of polyurethanes and polyisocyanurate with and without flame retardant: compounds of interest for chemical recycling, *J. Anal. Appl. Pyrol.* 160 (2021) 105374, <https://doi.org/10.1016/J.JAAP.2021.105374>.
- [60] J. Proano-Aviles, J.K. Lindstrom, P.A. Johnston, R.C. Brown, Heat and mass transfer effects in a furnace-based microreactor, *Energy Technol.* 5 (2017) 189–195, <https://doi.org/10.1002/ENTE.201600279>.
- [61] T. Shin, O. Hajima, W. Chuichi, Part 2 – pyrograms and thermograms of 163 high polymers, and MS data of the major pyrolyzates, in: *Pyrolysis – GC/MS Data B. Synth. Polym. Pyrograms, Thermograms MS Pyrolyzates*, Elsevier, 2011, pp. 7–335, <https://doi.org/10.1016/B978-0-444-53892-5.10002-1>.
- [62] J.Y. De Saint Laumer, E. Cicchetti, P. Merle, J. Egger, A. Chaintreau, Quantification in gas chromatography: prediction of flame ionization detector response factors from combustion enthalpies and molecular structures, in: *Anal. Chem.*, American Chemical Society, 2010, pp. 6457–6462, <https://doi.org/10.1021/ac1006574>.
- [63] P.J. Linstrom, W.G. Mallard, The NIST chemistry webbook: a chemical data resource on the internet, *J. Chem. Eng. Data* 46 (2001) 1059–1063, <https://doi.org/10.1021/JE000236I>.
- [64] Y. Nannoolal, J. Rarey, D. Ramjugernath, Estimation of pure component properties: Part 3. Estimation of the vapor pressure of non-electrolyte organic compounds via group contributions and group interactions, *Fluid Phase Equilib.* 269 (2008) 117–133, <https://doi.org/10.1016/J.FLUID.2008.04.020>.
- [65] A. Cuoci, A. Frassoldati, T. Faravelli, E. Ranzi, Numerical modeling of auto-ignition of isolated fuel droplets in microgravity, *Proc. Combust. Inst.* 35 (2015) 1621–1627, <https://doi.org/10.1016/J.PROCI.2014.06.035>.
- [66] E. Ranzi, T. Faravelli, F. Manenti, Pyrolysis, gasification, and combustion of solid fuels, in: *Adv. Chem. Eng.*, Academic Press, 2016, pp. 1–94, <https://doi.org/10.1016/bs.ache.2016.09.001>.
- [67] W.K. Metcalfe, S. Dooley, H.J. Curran, J.M. Simmie, A.M. El-Nahas, M. V. Navarro, Experimental and modeling study of C5H10O2 ethyl and methyl esters, *Chem. A Eur. J.* 111 (2007) 4001–4014, <https://doi.org/10.1021/jp067582c>.
- [68] H. Hippler, B. Viskolcz, Competition between alkyl radical addition to carbonyl bonds and H-atom abstraction reactions, *PCCP* 4 (2002) 4663–4668, <https://doi.org/10.1039/B201883G>.
- [69] B. Yang, C.K. Westbrook, T.A. Cool, N. Hansen, K. Kohse-Höinghaus, The effect of carbon-carbon double bonds on the combustion chemistry of small fatty acid esters, *S. Phys. Chem.* 225 (2011) 1293–1314, <https://doi.org/10.1524/zpch.2011.0167>.
- [70] H.J. Curran, Rate constant estimation for C1 to C4 alkyl and alkoxy radical decomposition, *Int. J. Chem. Kinet.* 38 (2006) 250–275, <https://doi.org/10.1002/KIN.20153>.
- [71] C.O. Rogers, K.S. Lockwood, Q.L.D. Nguyen, N.J. Labbe, Diol isomer revealed as a source of methyl ketene from propionic acid unimolecular decomposition, *Int. J. Chem. Kinet.* 53 (2021) 1272–1284, <https://doi.org/10.1002/KIN.21532>.
- [72] H. Ning, J. Wu, L. Ma, W. Ren, D.F. Davidson, R.K. Hanson, Combined Ab initio, kinetic modeling, and shock tube study of the thermal decomposition of ethyl formate, *Chem. A Eur. J.* 121 (2017) 6568–6579, <https://doi.org/10.1021/acs.jpca.7b05382>.
- [73] W. Sun, T. Tao, R. Zhang, H. Liao, C. Huang, F. Zhang, X. Zhang, Y. Zhang, B. Yang, Experimental and modeling efforts towards a better understanding of the high-temperature combustion kinetics of C3C5 ethyl esters, *Combust. Flame* 185 (2017) 173–187, <https://doi.org/10.1016/J.COMBUSTFLAME.2017.07.013>.
- [74] L. Coniglio, H. Bennadji, P.A. Glaude, O. Herbinet, F. Billaud, Combustion chemical kinetics of biodiesel and related compounds (methyl and ethyl esters): experiments and modeling – advances and future refinements, *Prog. Energy Combust. Sci.* 39 (2013) 340–382, <https://doi.org/10.1016/J.PECS.2013.03.002>.
- [75] R. Taylor, The mechanism of thermal elimination. Part 17. Rate data for pyrolysis of vinyl acetate and 1,2-diacetoxethane, *J. Chem. Soc. Perkin Trans. 2* (1983) 1157–1160, <https://doi.org/10.1039/P29830001157>.
- [76] A. Marongiu, T. Faravelli, E. Ranzi, Detailed kinetic modeling of the thermal degradation of vinyl polymers, *J. Anal. Appl. Pyrol.* 78 (2007) 343–362, <https://doi.org/10.1016/J.JAAP.2006.09.008>.
- [77] F. Serse, A. Bjola, M. Salvalaglio, M. Pelucchi, Unveiling solvent effects on  $\beta$ -scissions through metadynamics and mean force integration, *J. Chem. Theory Comput.* (2024), <https://doi.org/10.1021/ACS.JCTC.4C00383>.
- [78] B. Ruscic, R.E. Pinzon, M.L. Morton, G. von Laszewski, S.J. Bittner, S.G. Nijssure, K. A. Amin, M. Minkoff, A.F. Wagner, Introduction to active thermochemical tables: several “key” enthalpies of formation revisited, *Chem. A Eur. J.* 108 (2004) 9979–9997, <https://doi.org/10.1021/jp047912y>.
- [79] CRECK Modeling Lab, Kinetic-Mechanisms, (2024). <https://github.com/CRECKM/ODELING/Kinetic-Mechanisms> (accessed April 29, 2024).
- [80] P. Debiagi, T. Faravelli, C. Hasse, E. Ranzi, Kinetic modeling of solid, liquid and gas biofuel formation from biomass pyrolysis, in: Springer, Singapore, 2020, pp. 31–76, [https://doi.org/10.1007/978-981-15-2732-6\\_2](https://doi.org/10.1007/978-981-15-2732-6_2).
- [81] M. Dente, G. Bozzano, T. Faravelli, A. Marongiu, S. Pierucci, E. Ranzi, Kinetic modelling of pyrolysis processes in gas and condensed phase, *Adv. Chem. Eng.* 32 (2007) 51–166, [https://doi.org/10.1016/S0065-2377\(07\)32002-4](https://doi.org/10.1016/S0065-2377(07)32002-4).
- [82] E. Ranzi, M. Dente, A. Goldaniga, G. Bozzano, T. Faravelli, Lumping procedures in detailed kinetic modeling of gasification, pyrolysis, partial oxidation and combustion of hydrocarbon mixtures, *Prog. Energy Combust. Sci.* 27 (2001) 99–139, [https://doi.org/10.1016/S0360-1285\(00\)00013-7](https://doi.org/10.1016/S0360-1285(00)00013-7).
- [83] C. Hasse, P. Debiagi, X. Wen, K. Hildebrandt, M. Vascellari, T. Faravelli, Advanced modeling approaches for CFD simulations of coal combustion and gasification, *Prog. Energy Combust. Sci.* 86 (2021) 100938, <https://doi.org/10.1016/J.PECS.2021.100938>.
- [84] A. Locaspi, P. Debiagi, M. Pelucchi, C. Hasse, T. Faravelli, A predictive physico-chemical model of biochar oxidation, *Energy Fuel* 35 (2021) 14894–14912, <https://doi.org/10.1021/acs.energyfuels.1c01559>.
- [85] G. Ahmetli, S. Kocaman, I. Ozaytekin, P. Bozkurt, Epoxy composites based on inexpensive char filler obtained from plastic waste and natural resources, *Polym. Compos.* 34 (2013) 500–509, <https://doi.org/10.1002/PC.22452>.
- [86] J. Lee, T. Lee, Y.F. Tsang, J.I. Oh, E.E. Kwon, Enhanced energy recovery from polyethylene terephthalate via pyrolysis in CO<sub>2</sub> atmosphere while suppressing acidic chemical species, *Energy Convers. Manag.* 148 (2017) 456–460, <https://doi.org/10.1016/J.ENCONMAN.2017.06.026>.
- [87] F. Atashi, M. Gholizadeh, F. Ataei, Pyrolysis of bottle-grade polyethylene terephthalate: effect of carrier gases on carriage of pyrolysis products, *Polym. Eng. Sci.* 62 (2022) 2524–2531, <https://doi.org/10.1002/PEN.26025>.

- [88] E. Ranzi, A. Cuoci, T. Faravelli, A. Frassoldati, G. Migliavacca, S. Pierucci, S. Sommariva, Chemical kinetics of biomass pyrolysis, *Energy Fuel* 22 (2008) 4292–4300, <https://doi.org/10.1021/ef800551t>.
- [89] X. Zou, P. Debiagi, M.A. Amjed, M. Zhai, T. Faravelli, Impact of high-temperature biomass pyrolysis on biochar formation and composition, *J. Anal. Appl. Pyrol.* 179 (2024) 106463, <https://doi.org/10.1016/j.jaap.2024.106463>.
- [90] A. Locaspi, M. Pelucchi, M. Mehl, T. Faravelli, Towards a lumped approach for solid plastic waste gasification: polyethylene and polypropylene pyrolysis, *Waste Manag.* 156 (2022) 107–117, <https://doi.org/10.1016/j.wasman.2022.11.028>.
- [91] P. Morsch, M. Döntgen, K.A. Heufer, High- and low-temperature ignition delay time study and modeling efforts on vinyl acetate, *Proc. Combust. Inst.* 39 (2023) 115–123, <https://doi.org/10.1016/j.proci.2022.07.058>.
- [92] K. Murata, K. Sato, Y. Sakata, Effect of pressure on thermal degradation of polyethylene, *J. Anal. Appl. Pyrol.* 71 (2004) 569–589, <https://doi.org/10.1016/j.jaap.2003.08.010>.
- [93] H. Bennadji, L. Coniglio, F. Billaud, R. Bounaceur, V. Warth, P.A. Glaude, F. Battin-Leclerc, Oxidation of small unsaturated methyl and ethyl esters, *Int. J. Chem. Kinet.* 43 (2011) 204–218, <https://doi.org/10.1002/KIN.20536>.
- [94] E. Ranzi, M. Dente, T. Faravelli, G. Bozzano, S. Fabini, R. Nava, V. Cozzani, L. Tognotti, Kinetic modeling of polyethylene and polypropylene thermal degradation, *J. Anal. Appl. Pyrol.* 40–41 (1997) 305–319, [https://doi.org/10.1016/S0165-2370\(97\)00032-6](https://doi.org/10.1016/S0165-2370(97)00032-6).
- [95] A.M. El-Nahas, M.V. Navarro, J.M. Simmie, J.W. Bozzelli, H.J. Curran, S. Dooley, W. Metcalfe, Enthalpies of formation, bond dissociation energies and reaction paths for the decomposition of model biofuels: ethyl propanoate and methyl butanoate, *Chem. A Eur. J.* 111 (2007) 3727–3739, <https://doi.org/10.1021/jp067413s>.
- [96] A.S. Carson, D.H. Fine, P. Gray, P.G. Laye, Standard enthalpies of formation of diphenyl oxalate and benzoic anhydride and some related bond dissociation energies, *J. Chem. Soc. B Phys. Org.* (1971) 1611–1615, <https://doi.org/10.1039/J29710001611>.
- [97] T.P. Eskay, P.F. Britt, A.C. Buchanan, Pyrolysis of aromatic carboxylic acids: potential involvement of anhydrides in retrograde reactions in low-rank coal, *Energy Fuel* 11 (1997) 1278–1287, <https://doi.org/10.1021/ef9700745>.
- [98] W.J. Liu, F.X. Zeng, H. Jiang, X.S. Zhang, Preparation of high adsorption capacity bio-chars from waste biomass, *Bioresour. Technol.* 102 (2011) 8247–8252, <https://doi.org/10.1016/j.biortech.2011.06.014>.
- [99] E. Ranzi, P.E.A. Debiagi, A. Frassoldati, Mathematical modeling of fast biomass pyrolysis and bio-oil formation. Note I: kinetic mechanism of biomass pyrolysis, *ACS Sustain. Chem. Eng.* 5 (2017) 2867–2881, <https://doi.org/10.1021/acsschemeng.6b03096>.
- [100] S. Namysl, M. Pelucchi, O. Herbinet, A. Frassoldati, T. Faravelli, F. Battin-Leclerc, A first evaluation of butanoic and pentanoic acid oxidation kinetics, *Chem. Eng. J.* 373 (2019) 973–984, <https://doi.org/10.1016/j.cej.2019.05.090>.
- [101] C. Cavallotti, M. Pelucchi, A. Frassoldati, Analysis of acetic acid gas phase reactivity: rate constant estimation and kinetic simulations, *Proc. Combust. Inst.* 37 (2019) 539–546, <https://doi.org/10.1016/j.proci.2018.06.137>.
- [102] G. da Silva, G. da Silva, Carboxylic acid catalyzed keto-enol tautomerizations in the gas phase, *Angew. Chem.* 122 (2010) 7685–7687, <https://doi.org/10.1002/ANGE.201003530>.
- [103] H.K. Reimschuessel, Poly(ethylene terephthalate) formation. Mechanistic and kinetic aspects of direct esterification process, *Ind. Eng. Chem. Prod. Res. Dev.* 19 (1980) 117–125, <https://doi.org/10.1021/i360073a027>.
- [104] S.W. Benson, Thermochemical kinetics, 1976. [https://doi.org/10.1016/0022-2860\(70\)85028-1](https://doi.org/10.1016/0022-2860(70)85028-1).
- [105] E. Grajales-González, M. Monge-Palacios, S.M. Sarathy, Theoretical kinetic study of the unimolecular keto-enol tautomerism propen-2-ol -acetone. Pressure effects and implications in the pyrolysis of tert - and 2-butanol, *Chem. A Eur. J.* 122 (2018) 3547–3555, <https://doi.org/10.1021/ACS.JPCA.8B00836>.
- [106] M.V. Gil, J. Feroso, C. Pevida, J.J. Pis, F. Rubiera, Intrinsic char reactivity of plastic waste (PET) during CO<sub>2</sub> gasification, *Fuel Process. Technol.* 91 (2010) 1776–1781, <https://doi.org/10.1016/j.fuproc.2010.07.019>.
- [107] T. Faravelli, A. Frassoldati, G. Migliavacca, E. Ranzi, Detailed kinetic modeling of the thermal degradation of lignins, *Biomass Bioenergy* 34 (2010) 290–301, <https://doi.org/10.1016/j.biombioe.2009.10.018>.
- [108] D.W. Van Krevelen, *Properties of Polymers: Their Correlation with Chemical Structure; their Numerical Estimation and Prediction from Additive Group Contributions*, fourth ed., Elsevier, 2009.
- [109] M. Mehl, G. Vanhove, W.J. Pitz, E. Ranzi, Oxidation and combustion of the n-hexene isomers: a wide range kinetic modeling study, *Combust. Flame* 155 (2008) 756–772, <https://doi.org/10.1016/j.combustflame.2008.07.004>.
- [110] E. Ranzi, M. Dente, T. Faravelli, G. Pennati, Prediction of kinetic parameters for hydrogen abstraction reactions, *Combust. Sci. Technol.* 95 (1993) 1–50, <https://doi.org/10.1080/00102209408935325>.
- [111] D.C. Mielczarek, M. Matrat, A. Ben Amara, Y. Bouyou, P. Wund, L. Starck, Toward the accurate prediction of liquid phase oxidation of aromatics: a detailed kinetic mechanism for toluene autoxidation, *Energy Fuel* 31 (2017) 12893–12913, <https://doi.org/10.1021/acs.energyfuels.7b00416>.
- [112] C.A. Barson, J.C. Bevington, A tracer study of the benzyloxy radical, *Tetrahedron* 4 (1958) 147–156, [https://doi.org/10.1016/0040-4020\(58\)88013-8](https://doi.org/10.1016/0040-4020(58)88013-8).
- [113] L. Pratali Maffei, T. Faravelli, C. Cavallotti, M. Pelucchi, Electronic structure-based rate rules for H ipso addition–elimination reactions on mono-aromatic hydrocarbons with single and double OH/CH<sub>3</sub>/OCH<sub>3</sub>/CHO/C<sub>2</sub>H<sub>5</sub> substituents: a systematic theoretical investigation, *PCCP* 22 (2020) 20368–20387, <https://doi.org/10.1039/D0CP03099F>.
- [114] A. Nobili, A. Cuoci, W. Pejpichestakul, M. Pelucchi, C. Cavallotti, T. Faravelli, Modeling soot particles as stable radicals: a chemical kinetic study on formation and oxidation. Part I. Soot formation in ethylene laminar premixed and counterflow diffusion flames, *Combust. Flame* 243 (2022) 112073, <https://doi.org/10.1016/j.combustflame.2022.112073>.
- [115] C. Saggese, S. Ferrario, J. Camacho, A. Cuoci, A. Frassoldati, E. Ranzi, H. Wang, T. Faravelli, Kinetic modeling of particle size distribution of soot in a premixed burner-stabilized stagnation ethylene flame, *Combust. Flame* 162 (2015) 3356–3369, <https://doi.org/10.1016/j.combustflame.2015.06.002>.
- [116] W. Pejpichestakul, A. Frassoldati, A. Parente, T. Faravelli, Kinetic modeling of soot formation in premixed burner-stabilized stagnation ethylene flames at heavily sooting condition, *Fuel* 234 (2018) 199–206, <https://doi.org/10.1016/j.fuel.2018.07.022>.
- [117] W. Pejpichestakul, Chemical and Physical Pathways of PAH and Soot Formation in Laminar Flames, 2019.
- [118] M. Dente, G. Bozzano, G. Bussani, A comprehensive program for visbreaking simulation: product amounts and their properties prediction, *Comput. Chem. Eng.* 21 (1997) 1125–1134, [https://doi.org/10.1016/S0098-1354\(96\)00323-7](https://doi.org/10.1016/S0098-1354(96)00323-7).
- [119] D.S. Achilias, A review of modeling of diffusion controlled polymerization reactions, *Macromol. Theory Simul.* 16 (2007) 319–347, <https://doi.org/10.1002/MATS.200700003>.
- [120] T. Faravelli, M. Pincirol, F. Pisano, G. Bozzano, M. Dente, E. Ranzi, Thermal degradation of polystyrene, *J. Anal. Appl. Pyrol.* 60 (2001) 103–121, [https://doi.org/10.1016/S0165-2370\(00\)00159-5](https://doi.org/10.1016/S0165-2370(00)00159-5).
- [121] M. Pelucchi, A. Stagni, T. Faravelli, Addressing the complexity of combustion kinetics: data management and automatic model validation, *Comput. Aided Chem. Eng.* 45 (2019) 763–798, <https://doi.org/10.1016/B978-0-444-64087-1.00015-2>.
- [122] E. Ramalli, T. Dinelli, A. Nobili, A. Stagni, B. Pernici, T. Faravelli, Automatic validation and analysis of predictive models by means of big data and data science, *Chem. Eng. J.* 454 (2023) 140149, <https://doi.org/10.1016/j.cej.2022.140149>.
- [123] M.L. Poutsma, Reexamination of the pyrolysis of polyethylene: data needs, free-radical mechanistic considerations, and thermochemical kinetic simulation of initial product-forming pathways, *Macromolecules* 36 (2003) 8931–8957, <https://doi.org/10.1021/ma0303768>.
- [124] T. Faravelli, G. Bozzano, C. Scassa, M. Perego, S. Fabini, E. Ranzi, M. Dente, Gas product distribution from polyethylene pyrolysis, *J. Anal. Appl. Pyrol.* 52 (1999) 87–103, [https://doi.org/10.1016/S0165-2370\(99\)00032-7](https://doi.org/10.1016/S0165-2370(99)00032-7).
- [125] A. Ranzi, A. Frassoldati, M. Stagni, A. Pelucchi, T. Cuoci, E. Faravelli, A. Ranzi, A. Frassoldati, M. Stagni, A. Pelucchi, T.F. Cuoci, A. Ranzi, A. Frassoldati, M. Stagni, A. Pelucchi, T.F. Cuoci, Reduced kinetic schemes of complex reaction systems: fossil and biomass-derived transportation fuels, *Int. J. Chem. Kinet.* 46 (2014) 512–542, <https://doi.org/10.1002/kin.20867>.